PFC/RR-83-2 DOE/ET-51013-64 UC20 B,D

SECTOR GAP VOLTAGES AND INDUCED LOADS FOLLOWING PLASMA DISRUPTION IN FED/INTOR

BY

R.J. Thome, R.D. Pillsbury, Jr. and W.R. Mann

Massachusetts Institute of Technology
Plasma Fusion Center
Cambridge, Massachusetts 02139

December 1982

FOREWORD

This work was originally performed for the DOE, Office of Fusion Energy under a subcontract to the Fusion Engineering Design Center, Oak Ridge, Tennessee. Results were presented as part of the USA Contribution to the INTOR Workshop, (FED-INTOR/MAG/82-2), IAEA, Vienna, July 1982 and a condensed version was included in W.M. Stacey, Jr., M.A. Abdou, D.B. Montgomery, et al., "FED-INTOR, Critical Issues - Volume II", USA FED-INTOR/82-1, October 1982.

CONTENTS

1.0 INTRODUCTION

The rapid decay of magnetic flux associated with a plasma disruption induces voltages and currents in conducting bodies which are nearby. Recent tokamak designs utilize toroidal shells or shell segments near the plasma which are divided into sectors for assembly and maintenance purposes, but which may have electrically conducting paths toroidally in order to provide vacuum boundaries. The generation of voltage across sector gaps is a potential problem in the form of arc initiation with material damage. In addition, the induced currents interact with their own fields or fields from the TF or PF coils to generate electromagnetic loads which require consideration from the structural standpoint.

The examples presented in this report were generated as part of the FED/INTOR reactor design study[1] to illustrate the form and magnitude of these induced current effects and some of the machine characteristics which govern their behavior.

The rate at which the plasma flux decays and the strength of the induced current, fields and forces are dependent on the overall shell geometry since this governs the initial coupling with the plasma. The ability of the shells to carry net current through an rz-plane, that is, parallel to the initial plasma current, is also of fundamental importance. The magnitude of the interaction is then dependent on wall thickness and resistivity.

Section 2.0 presents the results from a finite element model of a multiple shell system for several cases involving shells capable of carrying net current, shells restricted to no net current and combinations of these cases. Field line patterns at selected instants after disruption

are given as well as plots of flux through the z = 0 plane in forms allowing cases to be compared. Results show that toroidal continuity to allow net current flow in partial shells or complete shells is an important ingredient for slowing down the initial rate of flux decay which is the source of the maximum voltage generated across sector gaps.

Simplified models for gap voltage estimation are described in Section 3.0. It is shown that very conservative models may yield results which are an order of magnitude higher than more accurate finite element models. The latter models become necessary if predictions based on the former substantially exceed design allowable levels. Examples related to INTOR and FED indicate that even if the two inner torus shells are sectored so that net toroidal current flow is prevented, gap voltages could be limited to 20 to 50 volts provided a third partial shell with toroidal continuity is used. Although there is considerable uncertainty concerning the allowable level for this voltage, the examples illustrate that design variations exist which can strongly influence its magnitude.

Section 4.0 considers the earlier cases from the standpoint of induced current and field decay time. Results indicate that considerable flexibility exists for adjustment of the decay rates and that rates are not described by a single exponential time constant. For a fixed shell geometry and set of restrictions on net current flow, decay times may be scaled proportional to the ratio of shell thickness to resistivity. Scaling in this way requires that all shells be scaled in the same way, that is, it does not apply if only a portion of the shell components are altered.

Section 5.0 presents the results for two cases based on the finite element model* to show the form and source of the net overturning moment

*The results for all cases were generated with a finite element, transient magnetic field program by Pillsbury.[2]

on a sector due to the interaction of the induced saddle currents, with the toroidal field. The eddy currents also lead to an equal and opposite twisting about the plasma axis at each end of the sector. Typical load levels for a FED/INTOR scale device are estimated to be nontrivial, but feasible for support.

2.0 PLASMA FLUX DECAY

This section will lay the groundwork for the discussion of induced voltages and shell time constants in the sections which follow. Both areas are strongly dependent on the manner in which the plasma flux links conducting shells in its vicinity and whether or not the shells can carry a net induced current in the toroidal direction.

Figure 1a shows a cross section of two toroidal shells in the rz-plane. Axial symmetry is assumed about the z-axis and symmetry is assumed relative to the z = 0 plane. The field lines from a uniform current density "plasma" of rectangular cross section are also shown. The field line patterns for a more realistic plasma current distribution would be somewhat different, but would not alter the general discussion or conclusions which follow. Figure 1a will be considered to be the steady-state, $t < 0$, condition. If the plasma current decays to zero in a time, t_d, as in a disruption, then eddy currents will be induced in the walls.

Figure 1b is identical to Fig. 1a except that a shaded region has been added to show that portion of the steady-state plasma flux which does not link any conducting material in the shells. This portion of the flux is

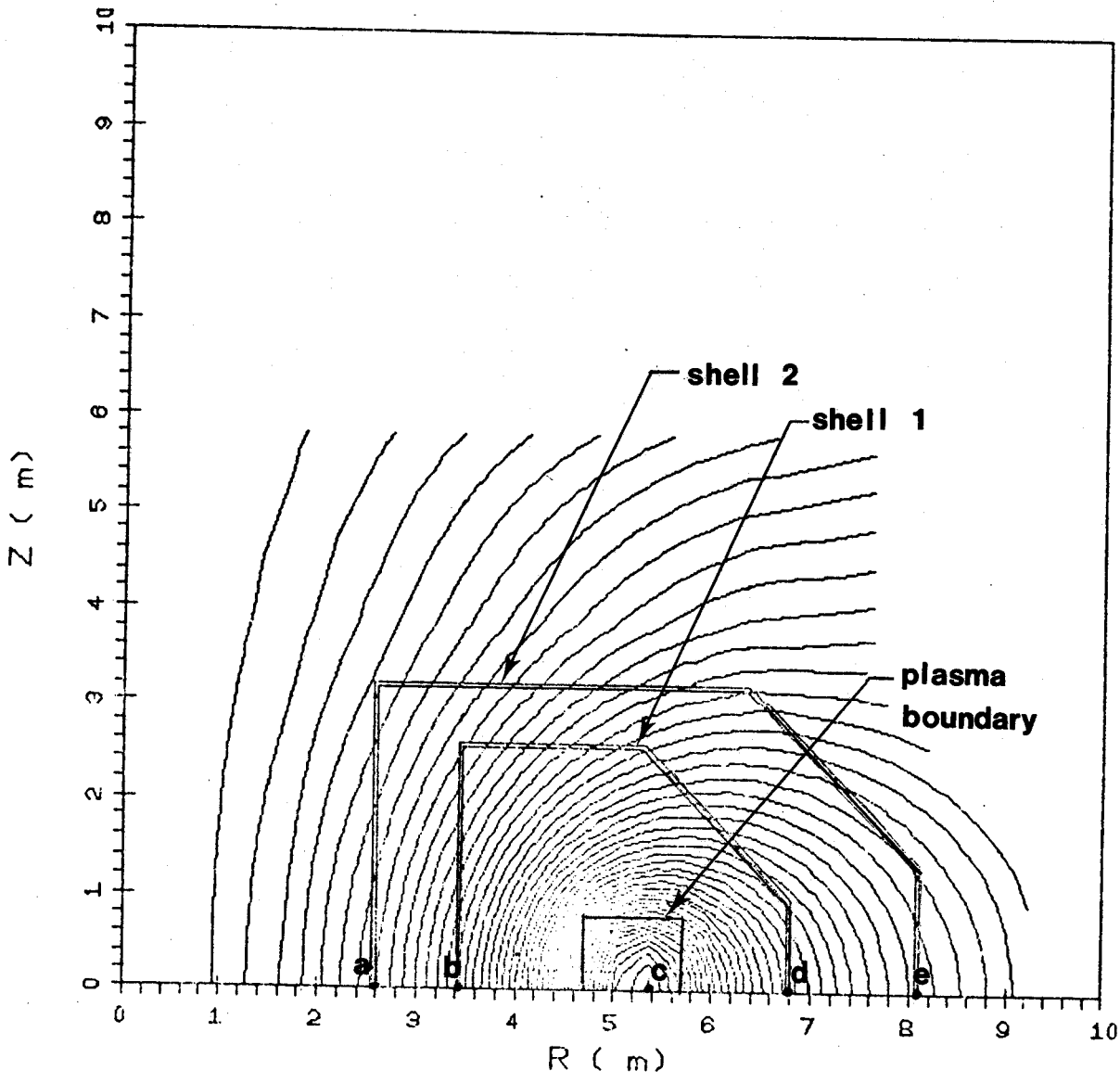

Figure 1a. Magnetic field lines produced by the plasma current, I_p, in the steady-state for $t < 0$.

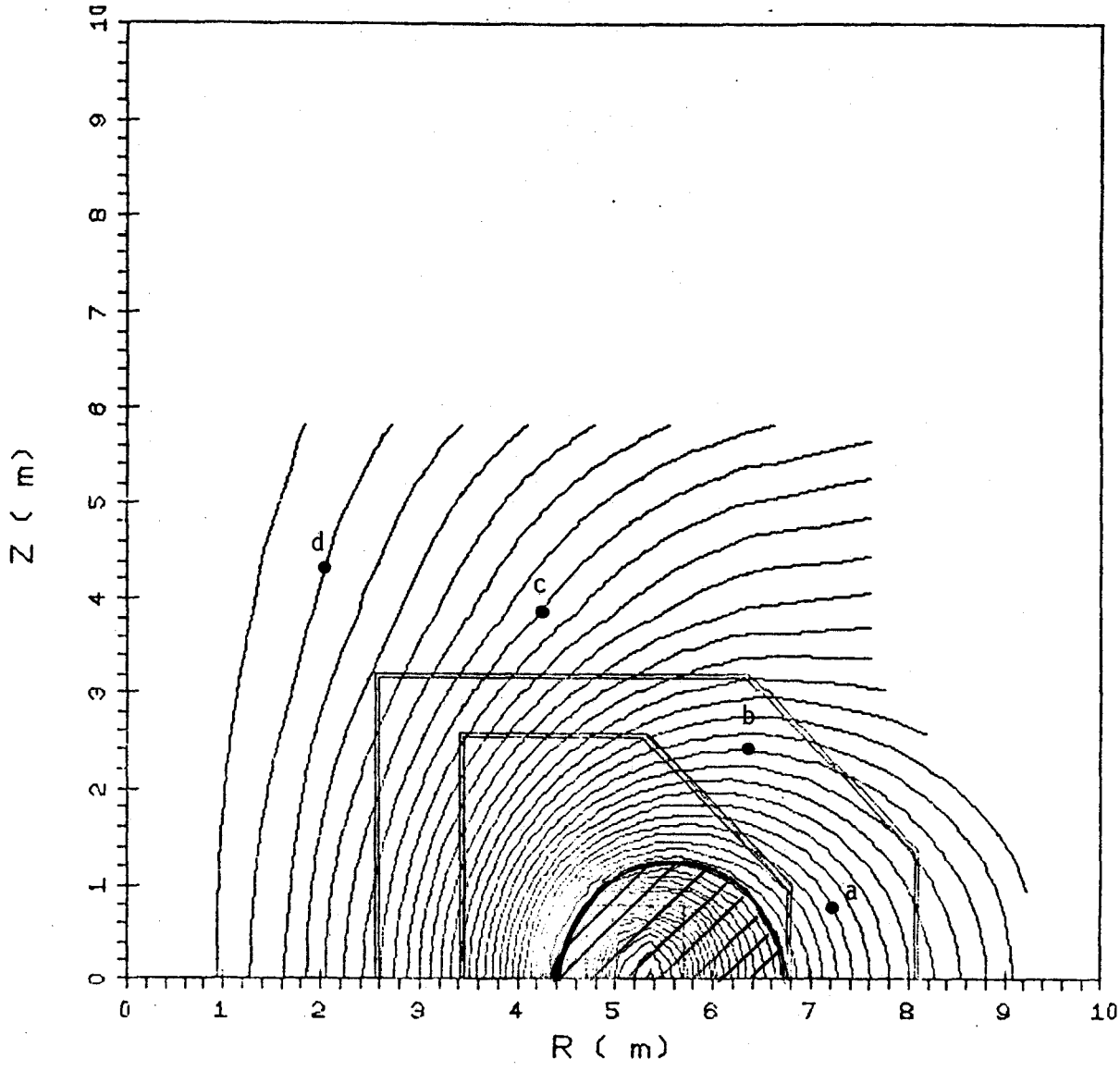

Figure 1b. Steady-state field lines for $t < 0$; the shaded region consists of field lines which do not link any shells.

not inductively coupled to the walls and can, therefore, collapse as the plasma current decays in the time, t_d. All other field lines either cut through shell 1 alone (e.g. - field line A), cut through both shells (e.g. - field line B), cut through shell 2 alone (e.g. - field line C), or link both shells by passing through the "hole" in the torus (e.g. - field line D) and, therefore, will be restrained in their attempts to move relative to the conducting material by the induced currents.

2.1 Shells With Net Current Flow

First, assume that both shells are electrically continuous in the toroidal direction. Hence, they are able to carry a net current through the rz-plane following the plasma disruption. Relatively thin, geometrically similar cases involving shells of this type would be expected to respond identically to a plasma current decay provided the shells had identical "magnetic Reynolds numbers" in the two cases. These parameters[3] are proportional to shell thickness and inversely proportional to shell resistivity and decay time for the driving current source. They represent the ratio of the characteristic time for diffusion of the field relative to the system to the characteristic decay time of the field source. Figures 2a and 2b illustrate field line patterns at two instants of time following a plasma current decay to zero in t_d = 0.010 s. Each shell has a thickness to resistivity ratio of $t_s/\rho = 4.12 \times 10^4\ \Omega^{-1}$ which corresponds to ~ 4 cm thick stainless steel. If, for example, the shells were ~ 0.08 cm thick copper, or ~ 0.13 cm thick aluminum then the patterns and results would be the same because t_s/ρ would be the same. Figure 2a shows that at 0.010 s there is essentially no change in the field pattern outside shell 1

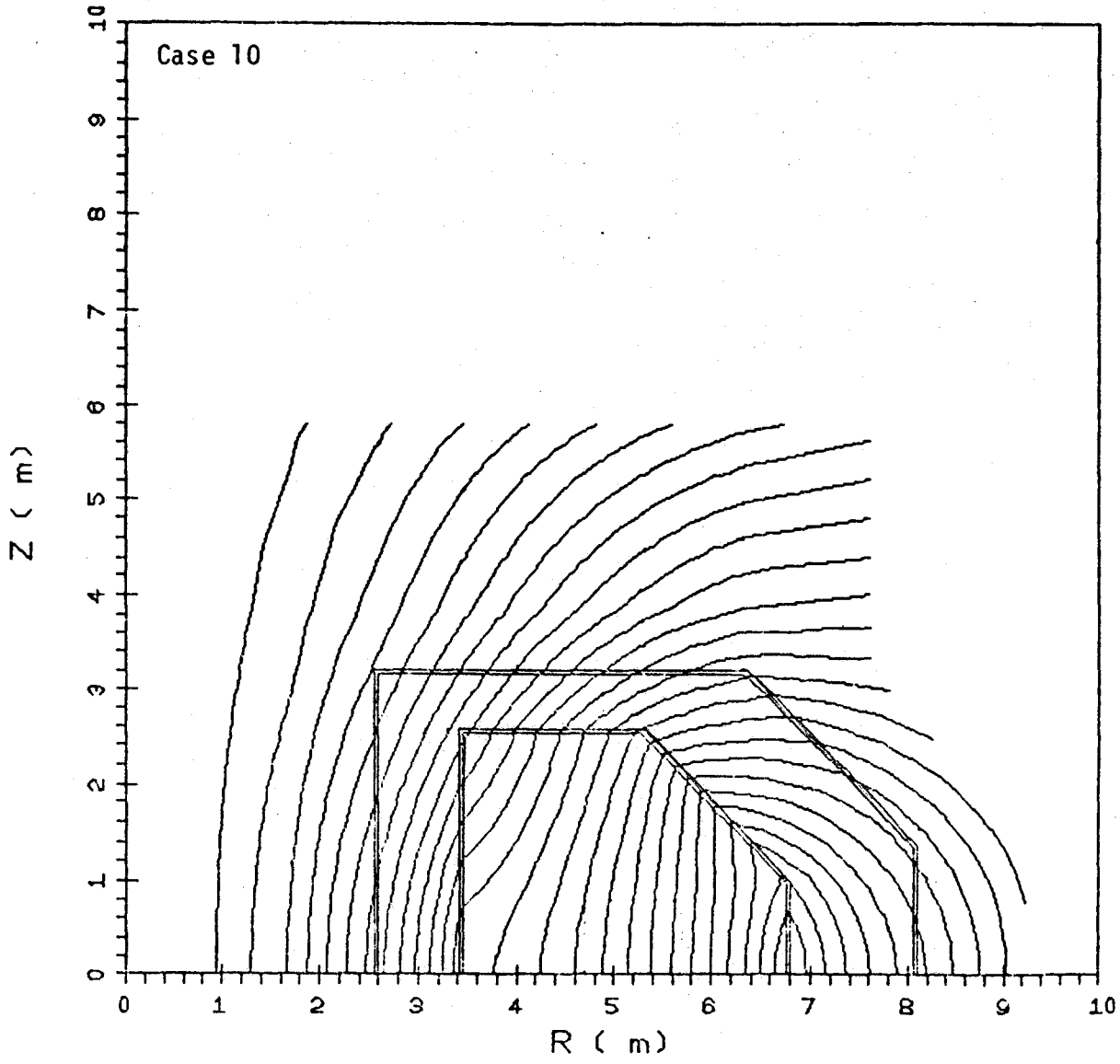

Figure 2a. Field lines at t = 0.010 sec for two shells capable of net current flow; induced currents flow primarily on the inner shell and the field pattern outside the first shell is essentially frozen ($t_s/\rho = 4.12 \times 10^4\ \Omega^{-1}$ for each shell).

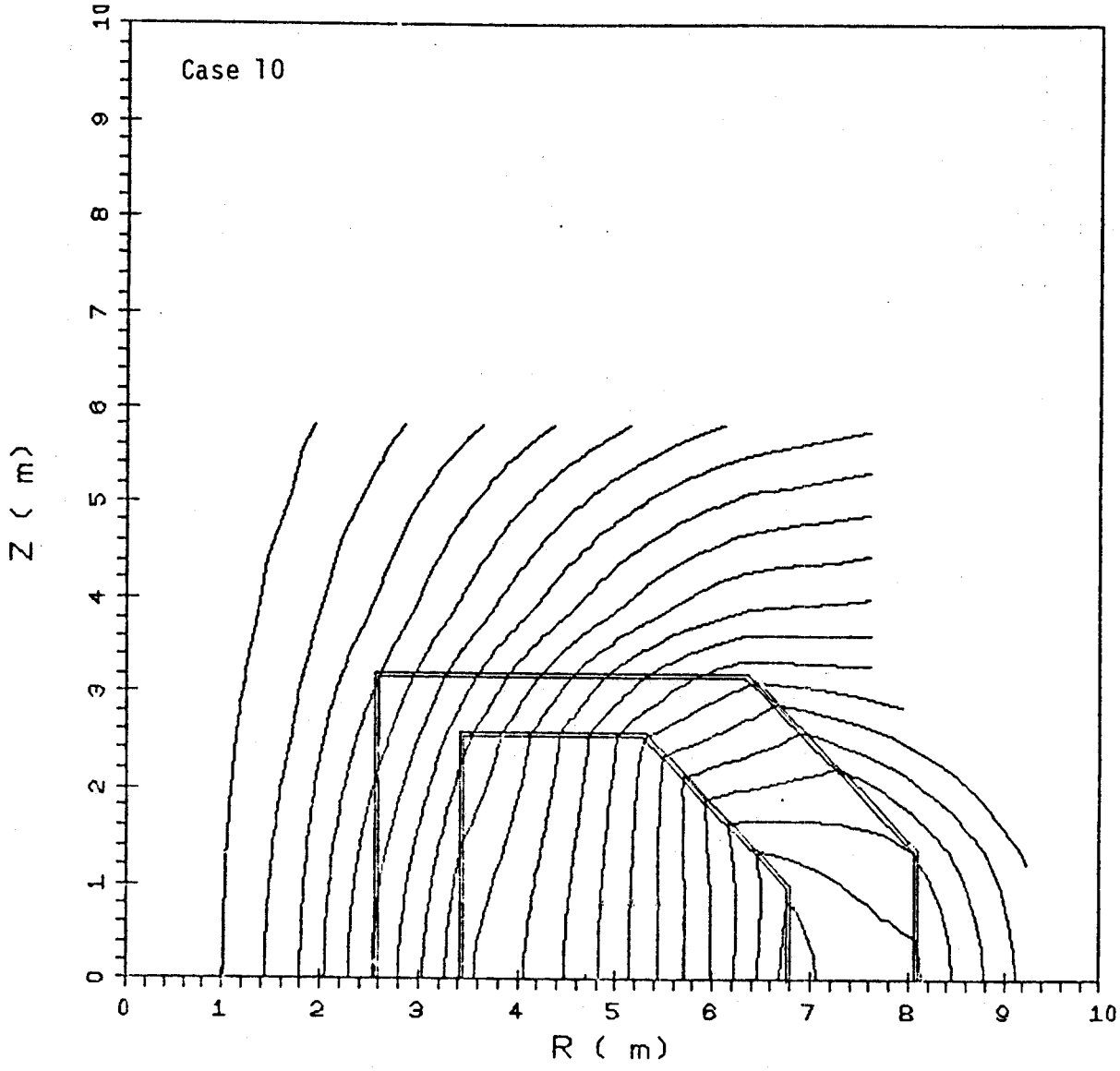

Figure 2b. Field lines at t = 0.05 sec for the shells in Fig. 2a; some current has now been induced in the outer shell near the outside of the torus.

(compare with Fig. 1a), indicating that the plasma current (i.e. - driving source) decay occurred on a time scale which was fast relative to the characteristic time for field diffusion through the shell. The presence of an induced current in a shell is implied in the figures by "kinks" in the field lines as they pass through the wall because a current sheet in the shell leads to a discontinuity in the tangential component of field at the shell. Note, then, that induced currents immediately following the disruption are concentrated on the inner shell since there are essentially no "kinks" in field lines passing through shell 2. The field line pattern within shell 1 has changed substantially because the uncoupled flux (i.e. - the shaded region in Fig. 1b) collapsed with the plasma current and the remaining flux within shell 1 was redistributed so as to satisfy $\nabla^2\bar{B} = 0$ in this region. Figure 2b shows the field lines at t = 0.050 s, when sufficient time has elapsed for the field disturbance to begin to diffuse through the inner wall and to induce significant currents in shell 2 as implied by the kinks in the field lines on the outboard side of the shell.

Further insight into the influence of the shells may be gained by considering Fig. 2c. The vertical axis is the net flux through the z = 0 plane versus radius for selected instants of time. Flux is given by

$$\Phi = \text{Flux} = 2\pi \int_0^r B_z(r, z = 0)\, r\,dr \qquad (1)$$

The flux at r = 0 is always zero and the maximum Φ for t < 0 occurs at point c which is located at the plasma current center (see Fig. 1a) because B_z is of different sign inboard and outboard of this point. The rapid decrease in plasma current and corresponding loss of the shaded flux in Fig. 1b in the same time interval, together with the redistribution of flux

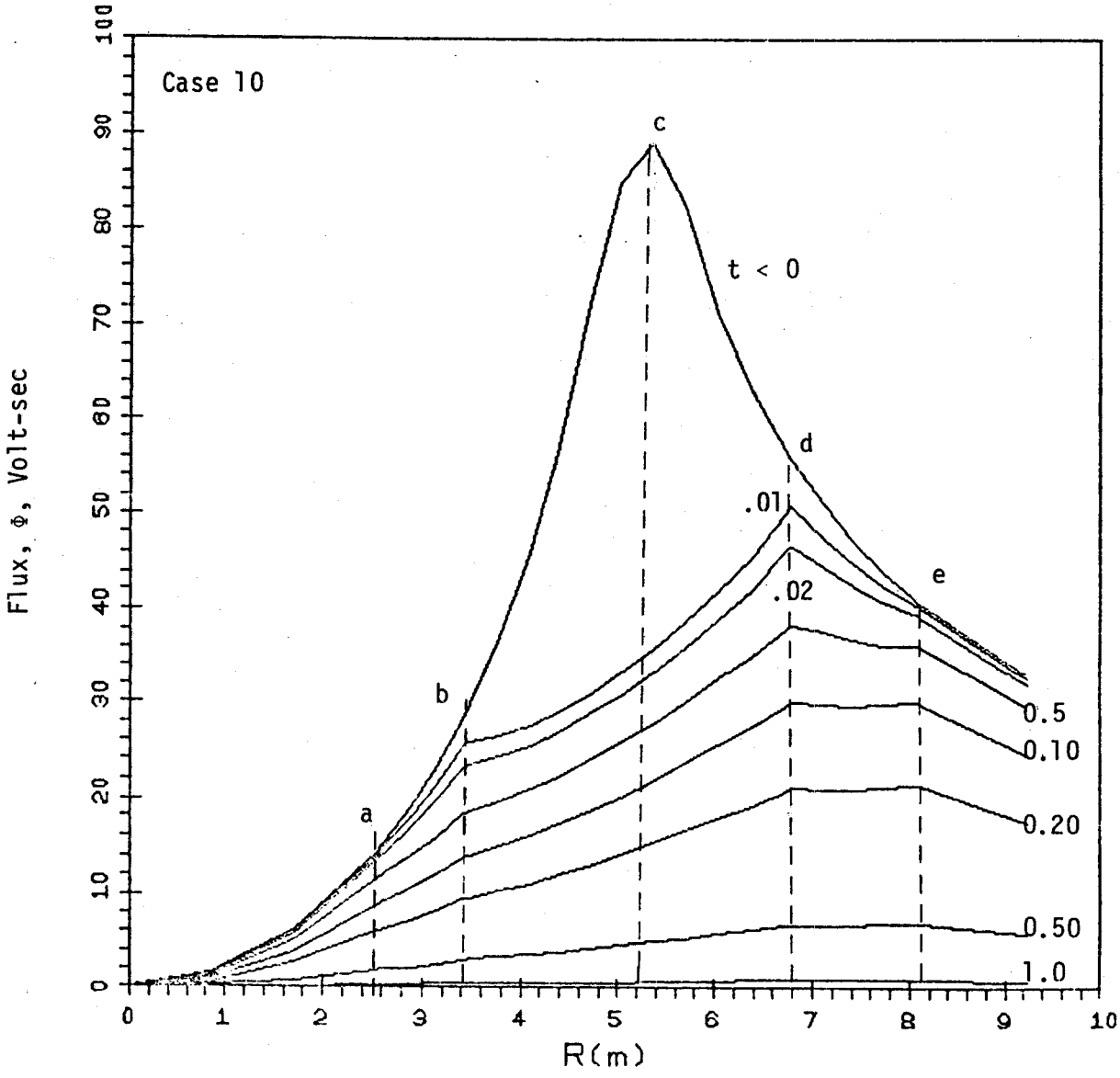

Figure 2c. Φ vs radius at selected instants of time in the z = 0 plane for two shells capable of net current flow as in Figure 2a (I_p = 5.4 MA; note: $\Phi \propto I_p$).

within shell 1, and small amount of diffusion through the shell, leads to the pattern indicated for t = 0.01 s. The subsequent decay of flux occurs on a longer time scale corresponding to induced current decay in the shells. The location of the shell intersections with the z = 0 plane (see, a,b,d,e in Fig. 1a) are also shown.

2.2 Shells With No Net Current

The t < 0 field pattern is produced by the plasma current, I_p, hence any closed contour in an rz-plane which encloses the plasma current must satisfy

$$\oint \bar{B} \cdot d\bar{c} = \mu_o I_p \tag{2}$$

If, for example, the contour is chosen along a field line outside both shells such as D in Fig. 1b and if the field along this contour is to be essentially unchanged before and after the plasma disruption then (2) implies that a net current of magnitude I_p must be induced through the rz-plane and within the contour immediately after the rapid plasma decay. Hence, the ability of the shells to sustain the flux in the region inboard of the plasma is tied to their ability to carry net current though the rz-plane.

Figure 3a is a schematic representation of the cross section of the shells in the z = 0 plane and shows that one or the other or both provide the ability to carry net current through an rz-plane if they are toroidally continuous. If, on the other hand, the shells are cut with radial planes and connected in sectors as schematically represented in Fig. 3b, then currents can still be induced in the shells following a plasma disruption.

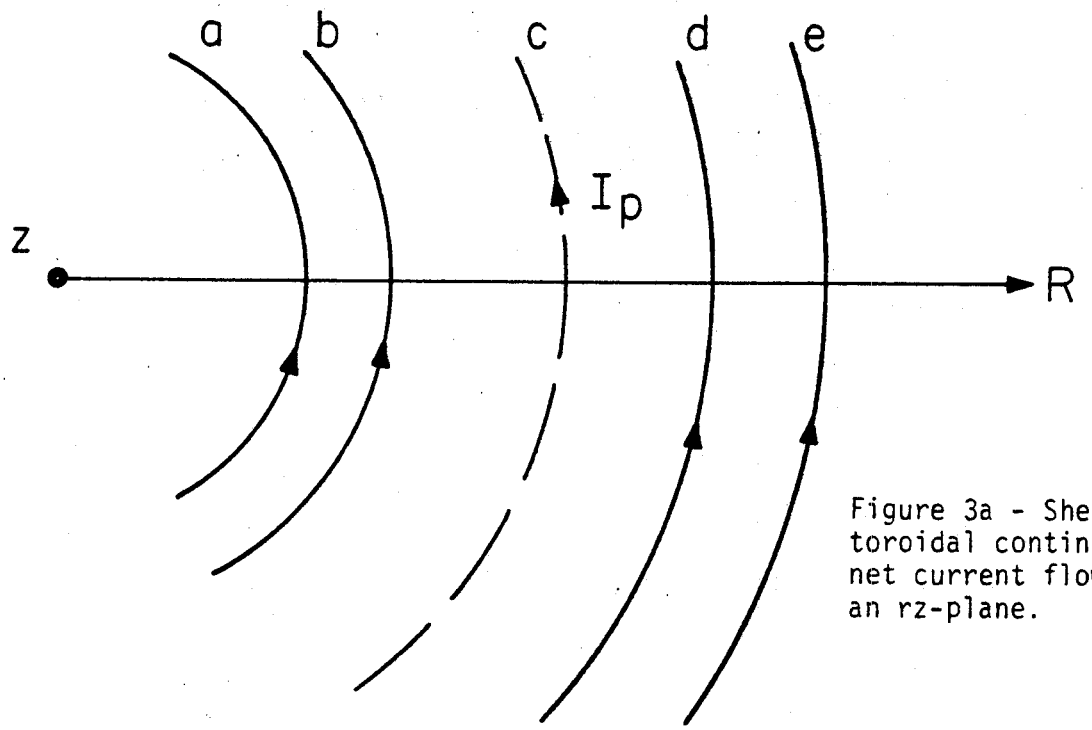

Figure 3a - Shells with toroidal continuity allow net current flow through an rz-plane.

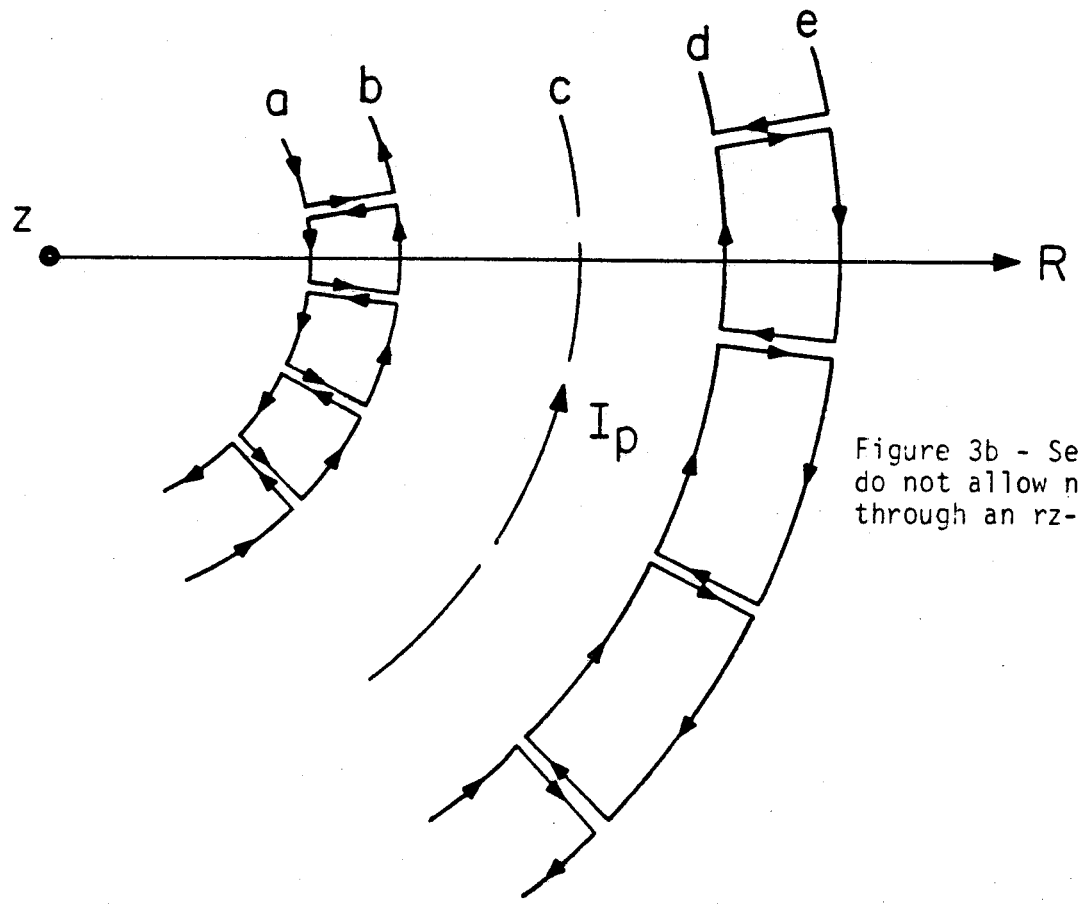

Figure 3b - Sectored shells do not allow net current flow through an rz-plane.

However, because there can be no net current flow through an rz-plane, Eq. (2) cannot be satisfied, thus we would expect a substantial change in the field pattern from those illustrated in Section 2.1. From another viewpoint, the change would be expected because of the substantial reduction in mutual inductance between the plasma and walls in Fig. 3b relative to the case in Fig. 3a.

Figures 4a to 4c show results for two shells assuming that the sum of the induced currents in both shells must be zero. Hence, the current at a point on a shell may return in the same shell or the other shell, but the sum of all currents through an rz-plane must be zero. Figures 4a to 4c are directly comparable with Figs. 2a to 2c in which net current flow was allowed. In Fig. 2a the field pattern outside shell 1 was essentially frozen in the $t < 0$ condition (see Fig. 1a) immediately following the disruption whereas in Fig. 4a, the only field lines which are frozen in the $t < 0$ condition are the field lines between shells. The field lines through the "hole" in the torus collapse during t_d since no net current is possible to sustain them. This point is emphasized by comparing Figs. 2c and 4c where the latter shows the initial collapse of flux throughout all space as well as in the vicinity of the plasma.

2.3 Combined Net and No Net Current Shells

First wall and shield boundaries in designs which have been considered recently often consist of combinations of cases allowing net current flow or restricting shells to no net current through an rz-plane. This section will, therefore, present three cases to illustrate typical effects.

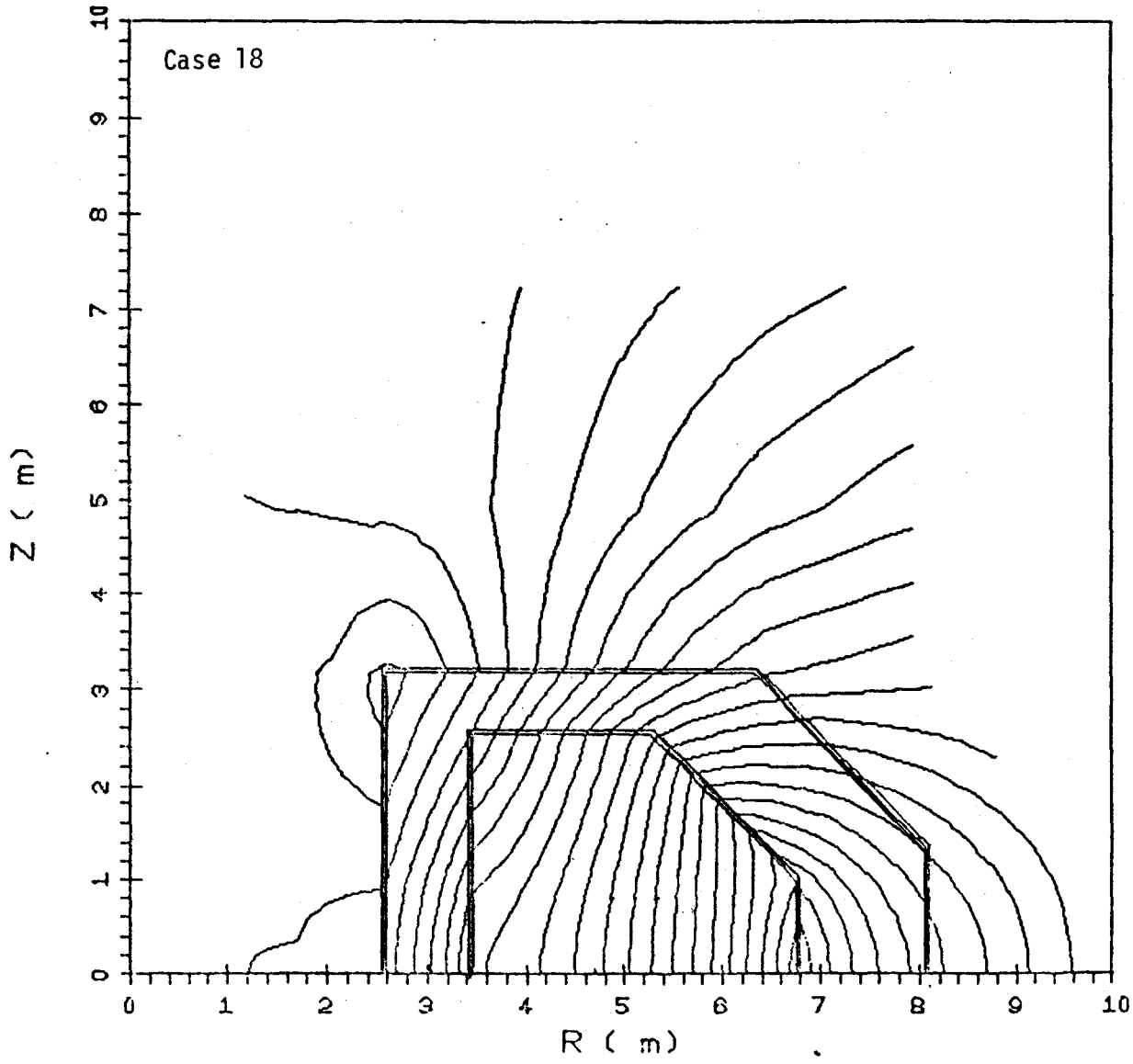

Figure 4a. Field lines at t = 0.010 sec for two shells restricted to no net current flow through the rz-plane; induced currents sustain the t < 0 flux pattern between shells, but the inability to produce a net current leads to substantial changes outside on the disruption time scale ($t_s/\rho = 4.12 \times 10^4\ \Omega^{-1}$ for each shell).

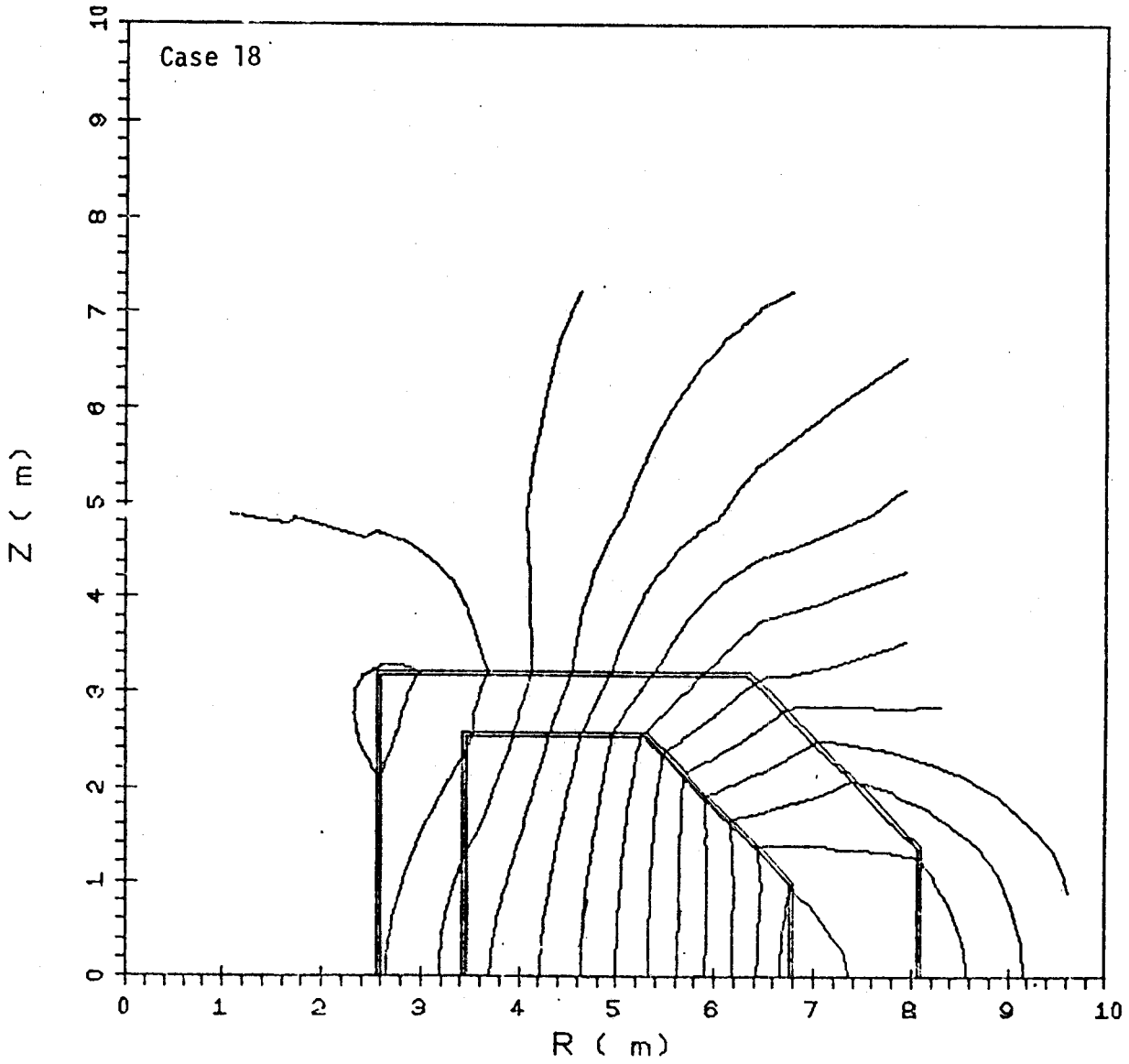

Figure 4b. Field lines at t = 0.05 sec for the shells in Figure 3a.

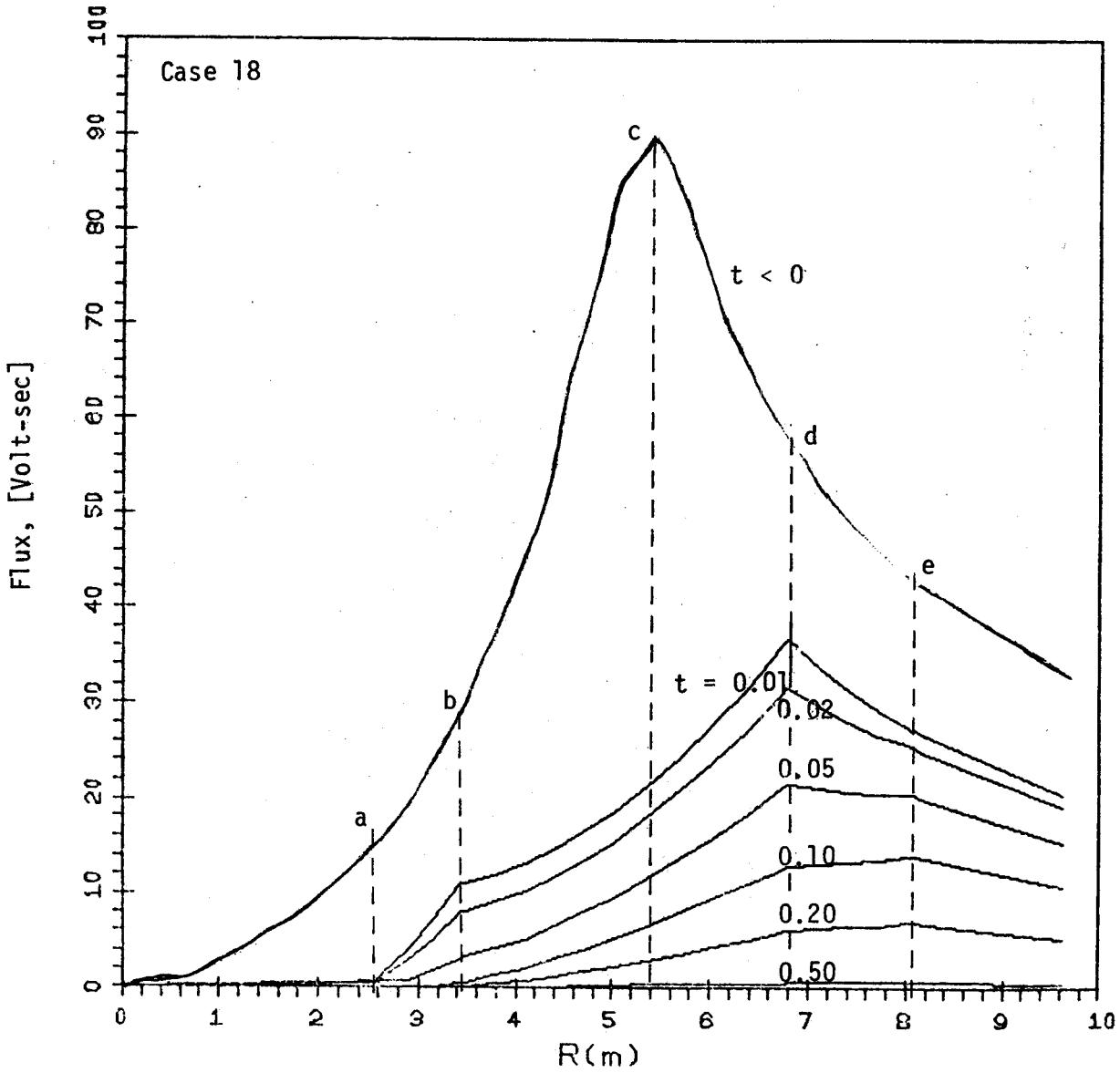

Figure 4c. Φ vs radius at selected instants of time in the z = 0 plane for two shells without net current flow as in Figure 3a. (I_p = 5.4 MA; note: $\Phi \propto I_p$).

The first case consists of three shells where shells 1 and 2 are identical to those in Fig. 4a in that they are restricted to no net current flow thus assuming they are sectored as illustrated in Fig. 3b. The third shell is adjacent to and on the outside of shell 2, but is assumed to be toroidally continuous and can thus carry current through the rz-plane. Each shell is assumed to have the same shell thickness to resistivity ratio, $t_s/\rho = 4.12 \times 10^4\ \Omega^{-1}$. Field lines are shown in Figs. 5a and 5b for times of 0.01 s and 0.05 s respectively and a flux plot is given in Fig. 5c. Comparison of these results with similar figures for the previous two cases illustrate the ability of the continuous, net current outer wall to sustain flux through the "hole" in the torus and restrain the initial rate of flux decay between points a and c relative to the two shell, no net current case in Fig. 4c. The inner shell is not quite as effective in slowing down the flux decay after the initial flux collapse as when it was continuous (compare Fig. 4c with the case in Fig. 2c.)

The case illustrated in Fig. 5 involved two sectored shells and one complete continuous outer shell which, for example, could be a vacuum boundary. In some design variations, a complete shell which is toroidally continuous does not lie close to the two sectored shells. Figure 6a for example, shows a configuration where the two shells are sectored and, therefore, cannot carry net current flow through the rz-plane and where there is a third, partial shell inboard which can carry net current (this is the case, for example, in "FED-81"[4] where the continuous shell is part of the spool). Figures 6a, 6b and 6c may be directly compared with earlier, similar figures to show that the inboard partial shell segment is quite

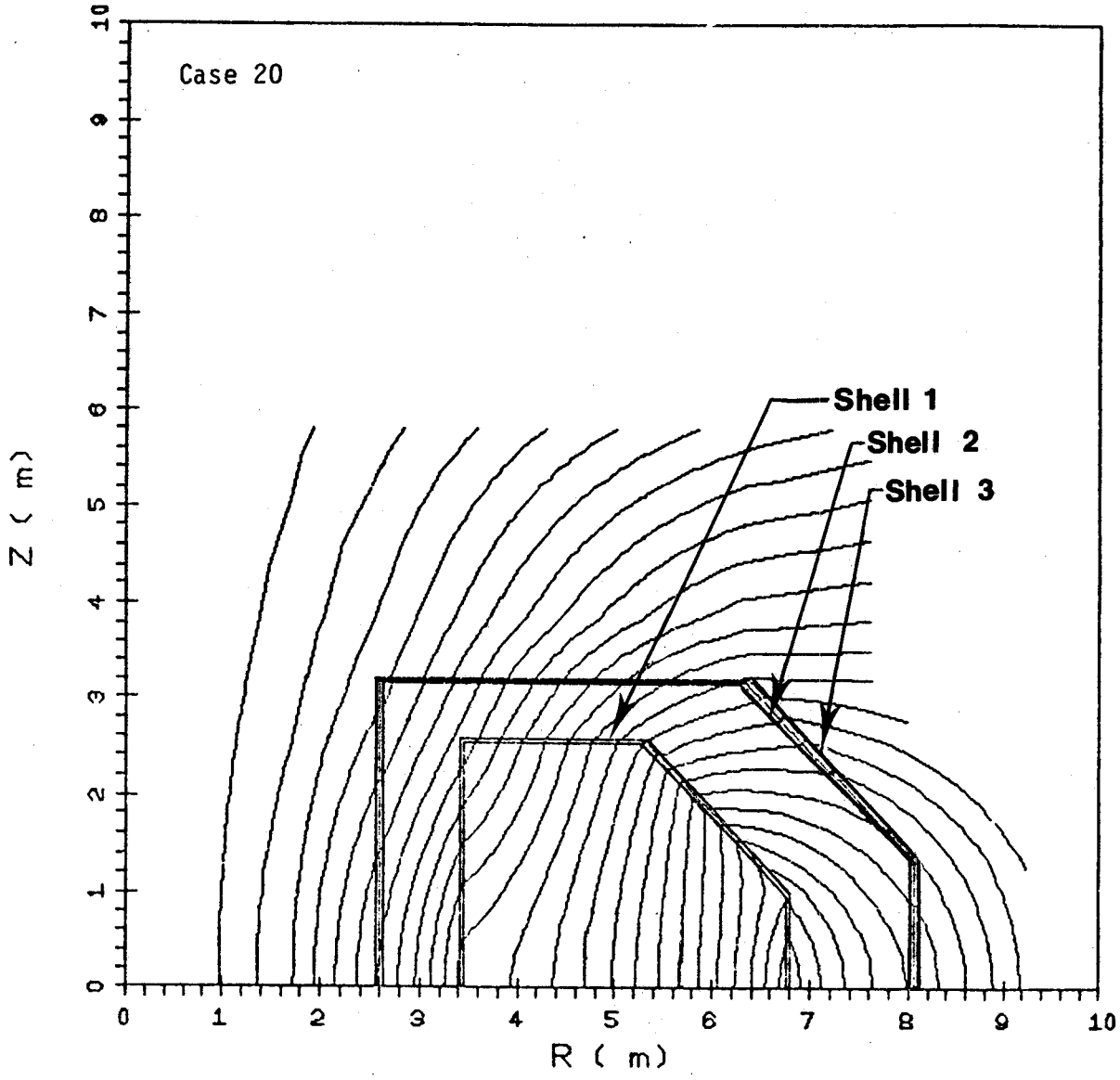

Figure 5a. Field lines at t = 0.010 sec for three shells where shells 1 and 2 are restricted to no net current and shell 3 is allowed to have net current flow through the rz-plane. ($t_s/\rho = 4.12 \times 10^4\ \Omega^{-1}$ for each shell).

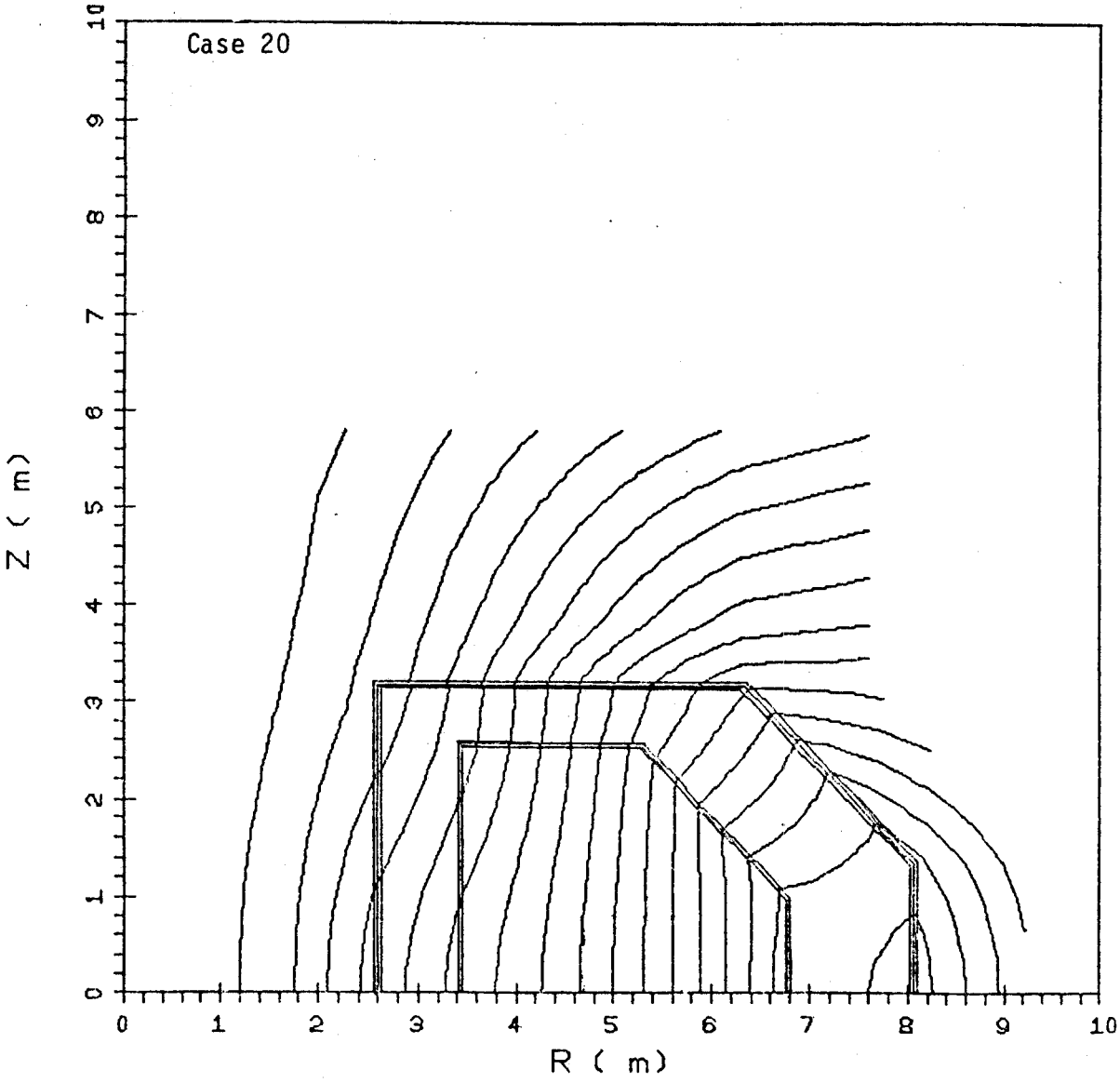

Figure 5b. Field lines at t = 0.050 sec for the three shells in Figure 5a.

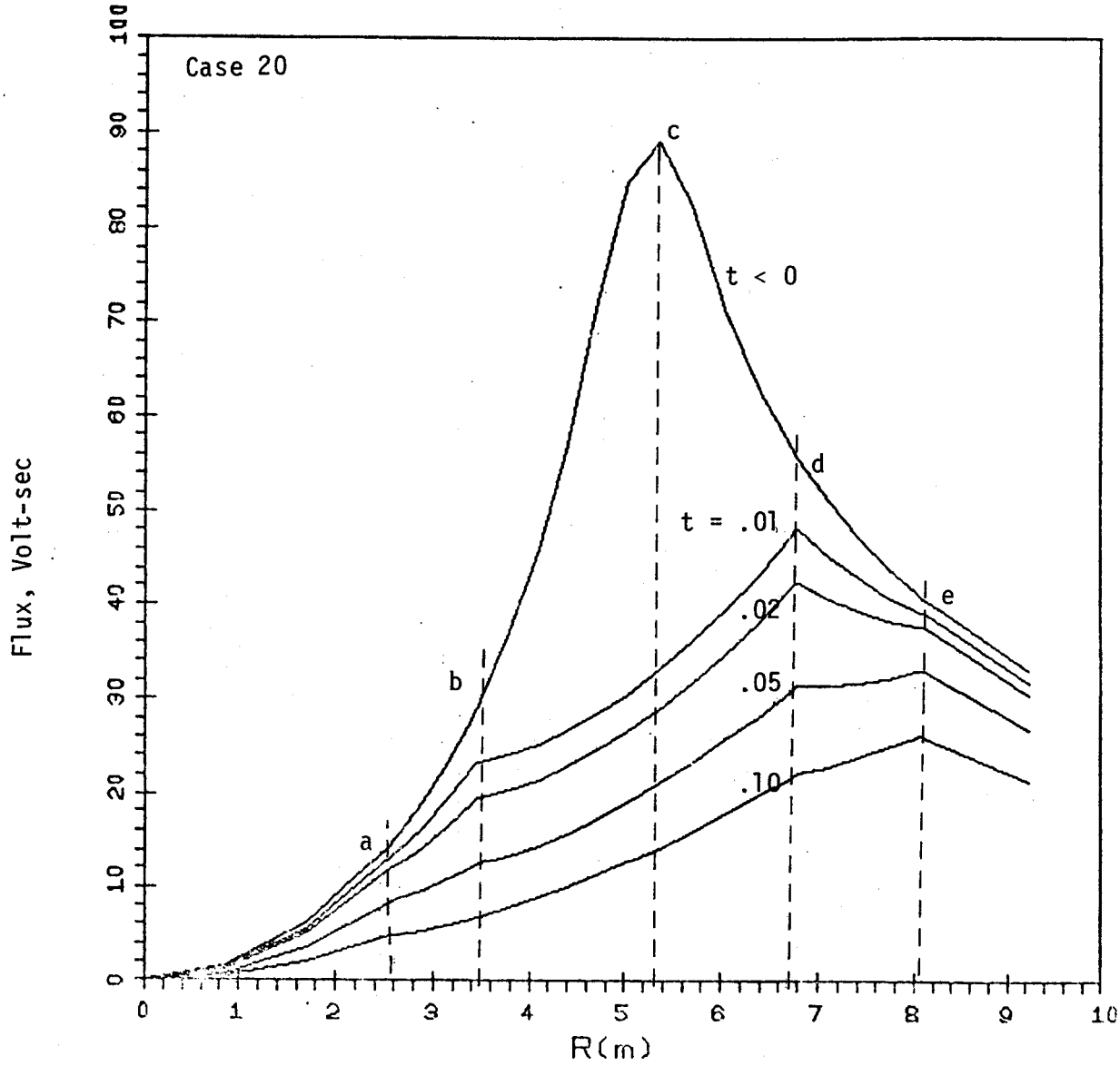

Figure 5c. Φ vs radius at selected instants of time in the z = 0 plane for three shells where shells 1 and 2 are restricted to no net current and shell 3 is allowed to have net current. (I_p = 5.4 MA; note: $\Phi \propto I_p$).

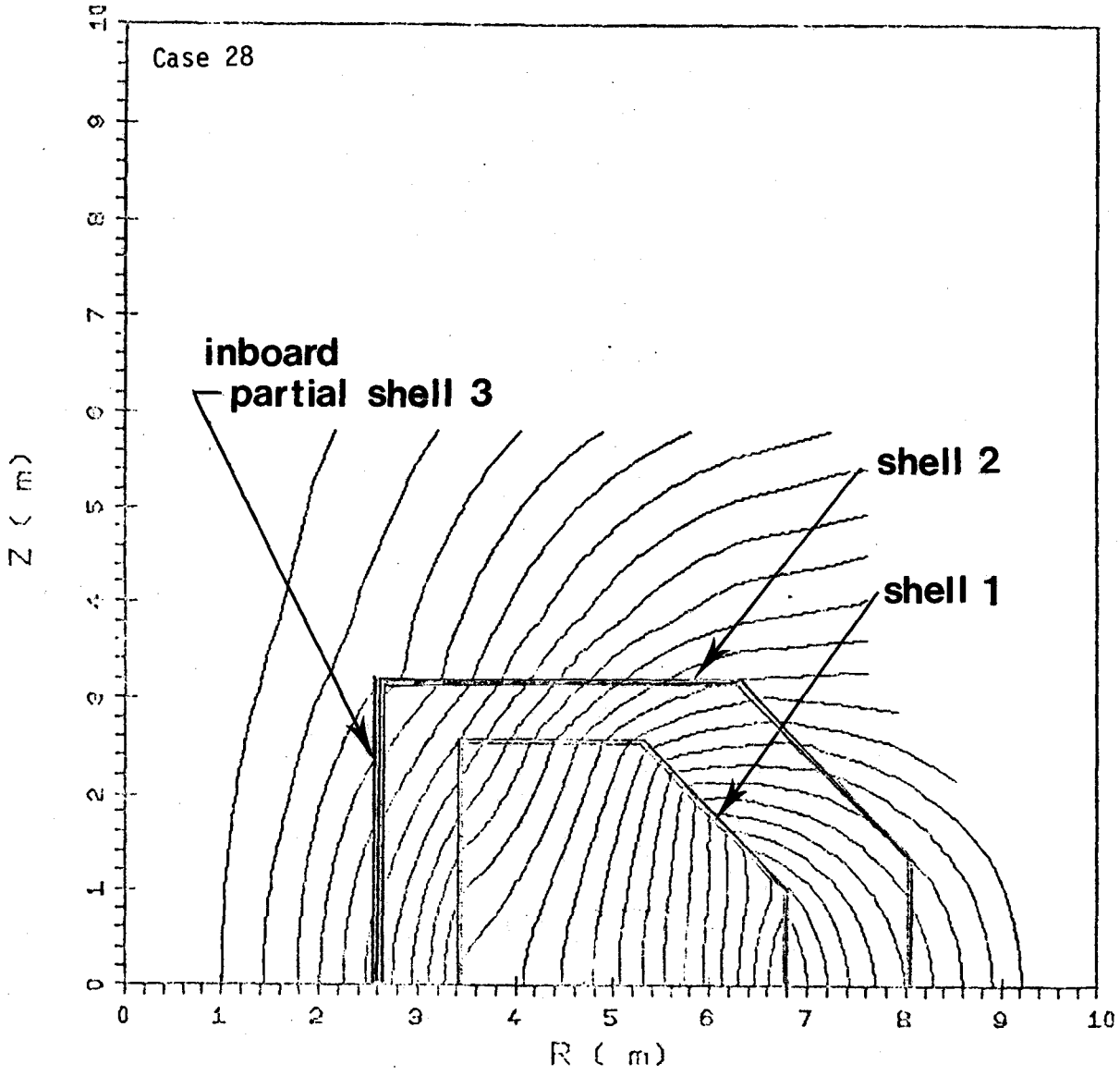

Figure 6a. Field lines at t = 0.010 sec for a partial shell inboard which can carry net current and shells 1 and 2 which are restricted to no net current through the rz-plane ($t_s/\rho = 4.2 \times 10^4\ \Omega^{-1}$ for each shell).

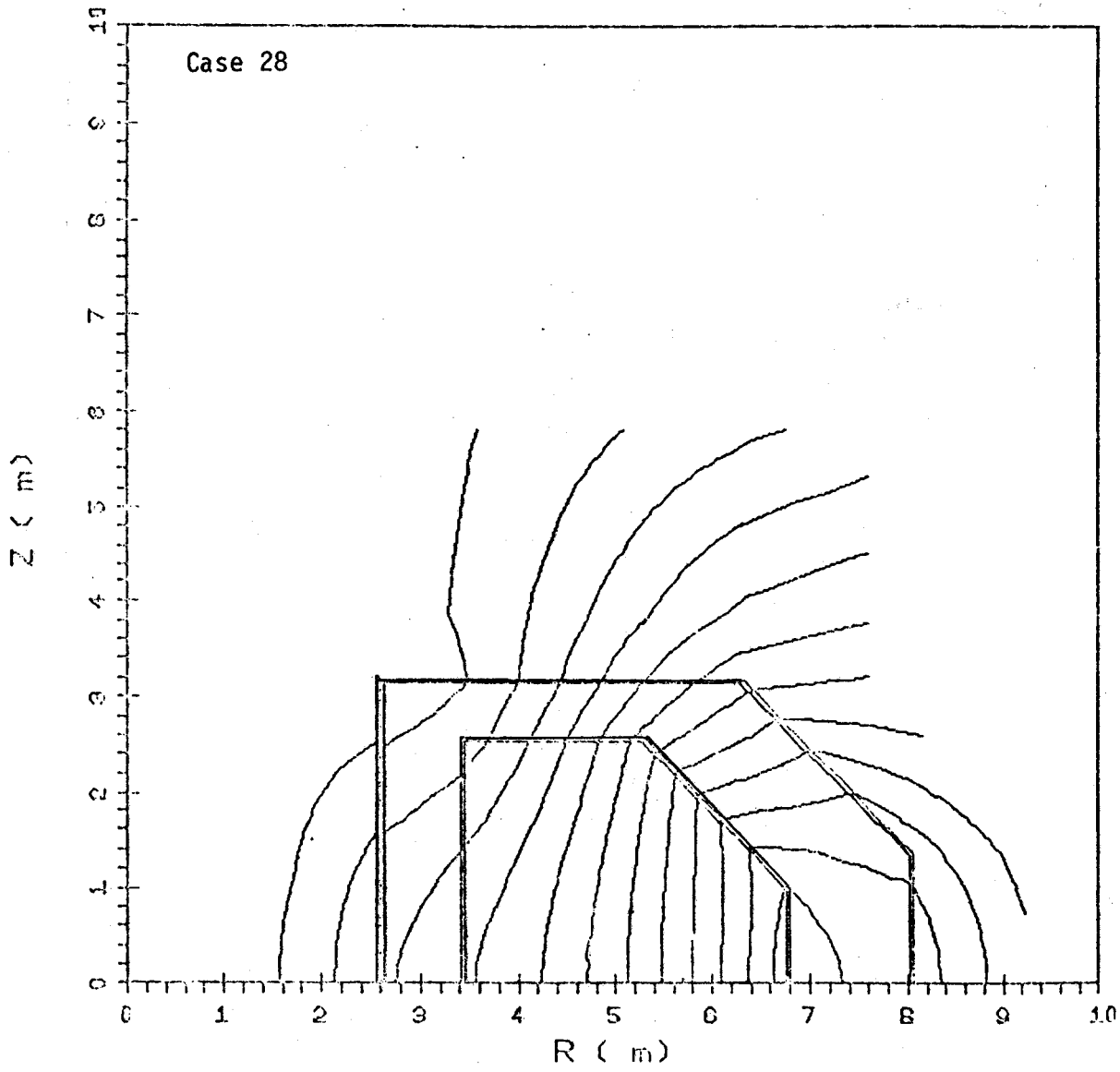

Figure 6b. Field lines at t = 0.050 sec for the shells in Figure 6a.

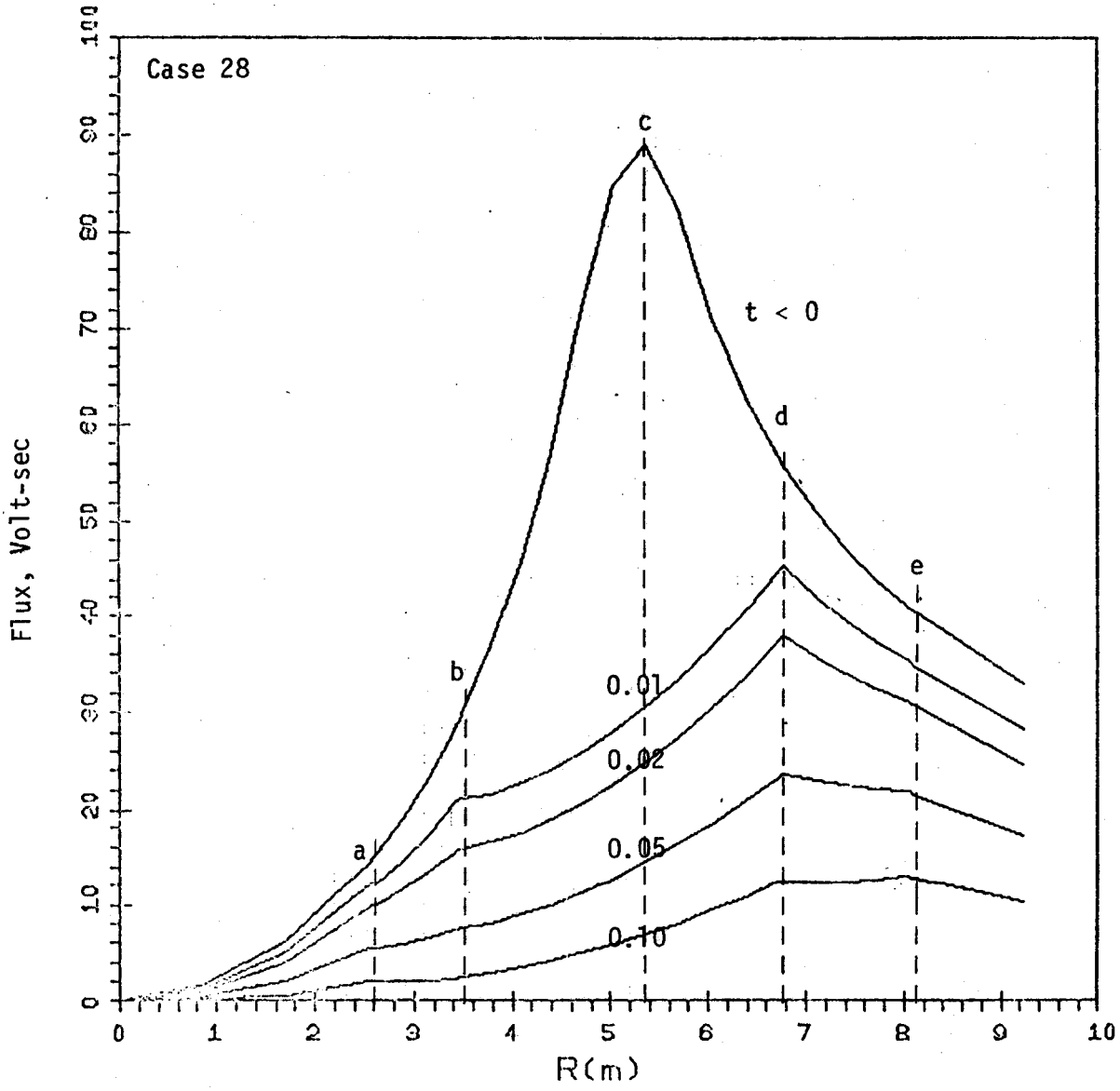

Figure 6c. Φ vs radius at selected instants of time in the z = 0 plane for shells 1 and 2 with no net current and a third partial shell inboard capable of net current flow (I_p = 5.4 MA; note: $\Phi \propto I_p$).

effective in decreasing the initial flux collapse because of its ability to carry net current to support the flux which originally passed through the "hole" in the torus.

The last case to be presented is similar to the configuration in Fig. 6 except that the continuous partial shell is located outboard rather than inboard. Results are shown in Fig. 7a to 7c and, when compared with Fig. 6 show that the outboard shell is not as effective since it allows a fraction of the bore flux to collapse along with the plasma current.

The results for cases presented in this section were generated using a finite element model of shells with overall dimensions comparable to those being considered for INTOR and FED.[1] They illustrate the importance of toroidal continuity of at least a portion of a shell to maintain a large fraction of the flux initially produced by the plasma. This has a significant effect on the sector gap voltages which are produced by the flux change during a disruption. The next section will show methods for estimating sector gap voltages and use results from this section to arrive at approximate voltage levels for these reactors.

3.0 SECTOR GAP VOLTAGES

First wall, blanket and shield designs which have been considered recently have included shells which may or may not be toroidally continuous. If they are sectored for ease of assembly and maintenance then questions arise concerning possible arcing across sector gaps due to the voltage induced by a disruption. The next section develops a simple model for

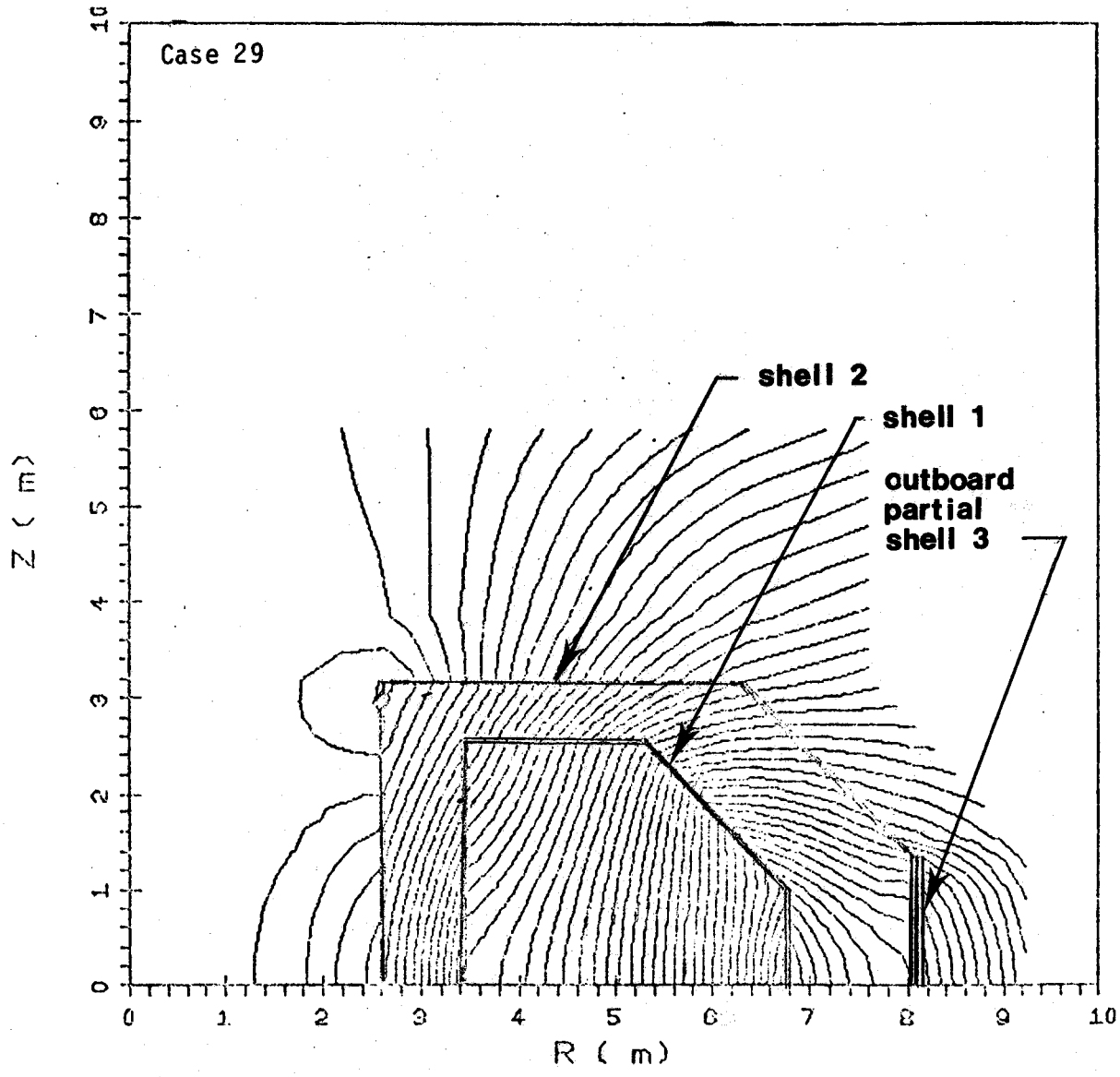

Figure 7a. Field lines at t = 0.010 sec for a partial shell outboard which can carry net current and shells 1 and 2 which are restricted to no net current through the rz-plane (t_s/ρ = 4.12 x 10^4 Ω^{-1} for each shell).

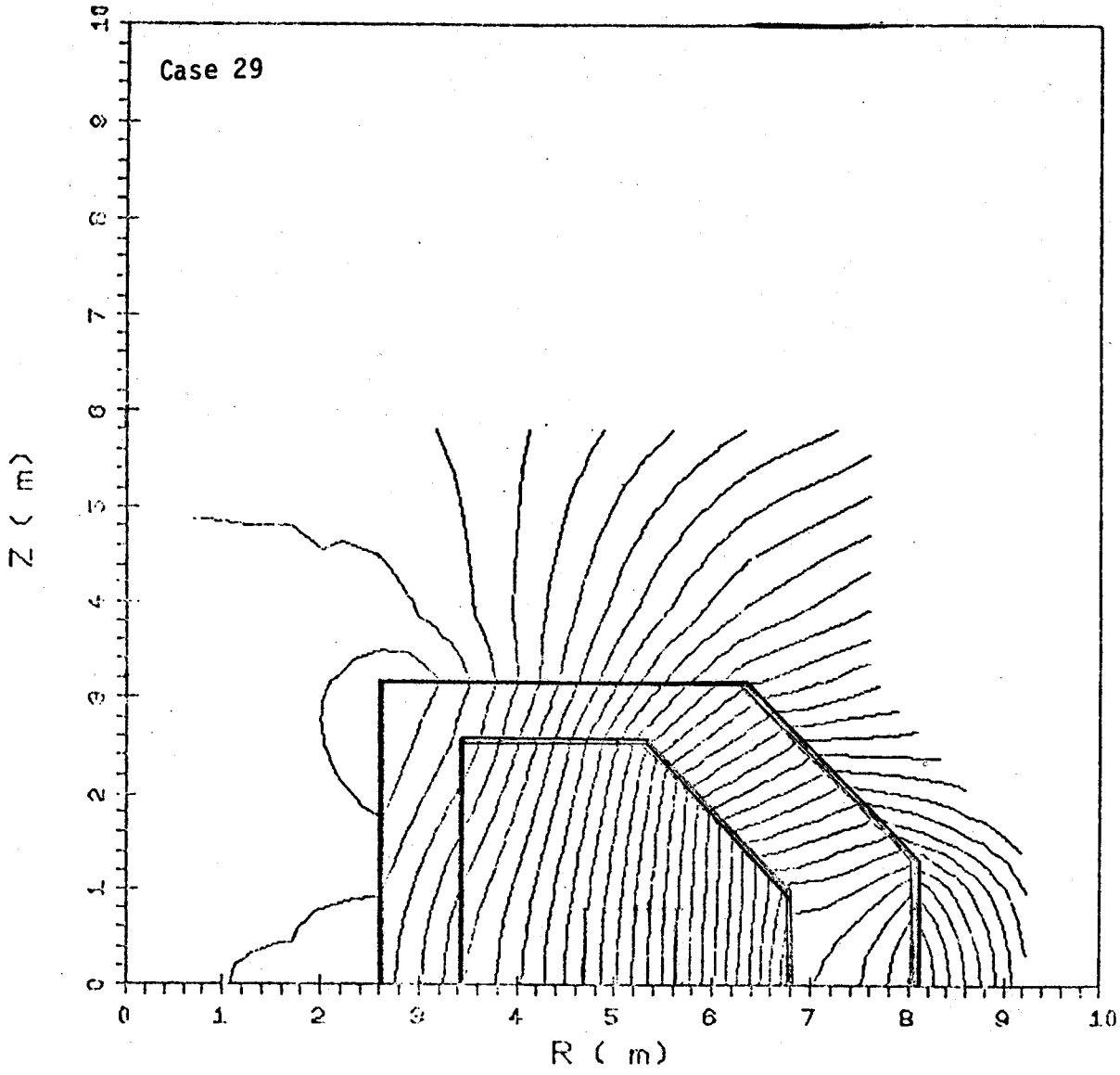

Figure 7b. Field lines at t = 0.050 sec for the shells in Figure 7a.

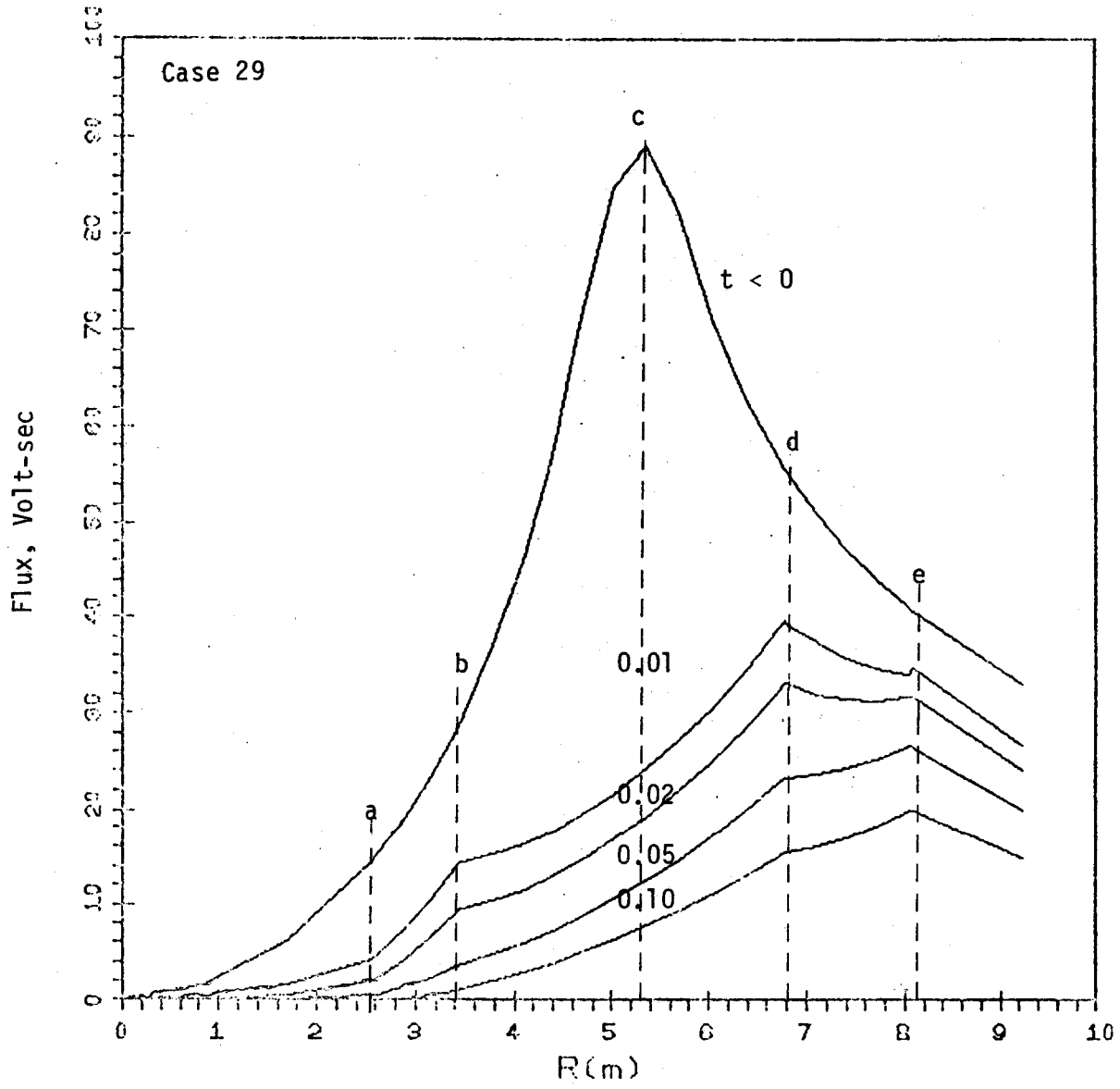

Figure 7c. Φ vs radius in the z = 0 plane at selected instants of time for shells 1 and 2 with no net current and a third partial shell outboard capable of net current flow (I_p = 5.4 MA; note: $\Phi \propto I_p$).

estimating the induced voltage distribution. This is then applied to examples for FED and INTOR in Section 3.2.

3.1 Maximum Voltage Estimation

The method for voltage estimation across sector gaps during a plasma disruption may be described with a series of simplified diagrams. Figure 8 shows two inductively coupled circuits. The plasma is represented by a single circular filament carrying a current I_p for $t < 0$. A wall or electrically conducting shell which is inductively coupled to the plasma is represented as a closed loop of resistors R carrying no current for $t < 0$. At $t = 0$ the plasma current decays to zero and induces a current I_w in the wall which then decays with a characteristic time constant for the loop. The driving voltage for the wall current is the instantaneous rate of change of flux linked by the wall. At any instant during the wall current decay, the net voltage drop between any two points A and B in the loop is zero provided the number of resistors is infinite and they are uniformly distributed. This is illustrated in Fig. 9 for a loop with a circumferential length, ℓ. Figure 9 is a voltage plot along the periphery and shows that, at any instant the distributed resistive and inductive voltages cancel to yield a net voltage of zero everywhere in the loop.

If we now assume that the number of resistors is 2n, that the inductance is still uniformly distributed, and, that the resistors are alternately small and large in magnitude, then the voltage distribution along the circumference at a given instant is as shown in Fig. 10. Figure 10 illustrates that the net voltage is still zero at points between each pair of resistors, but the linear inductive voltage distribution combines with the nonlinear resistive voltage to yield a "sawtooth" variation in net

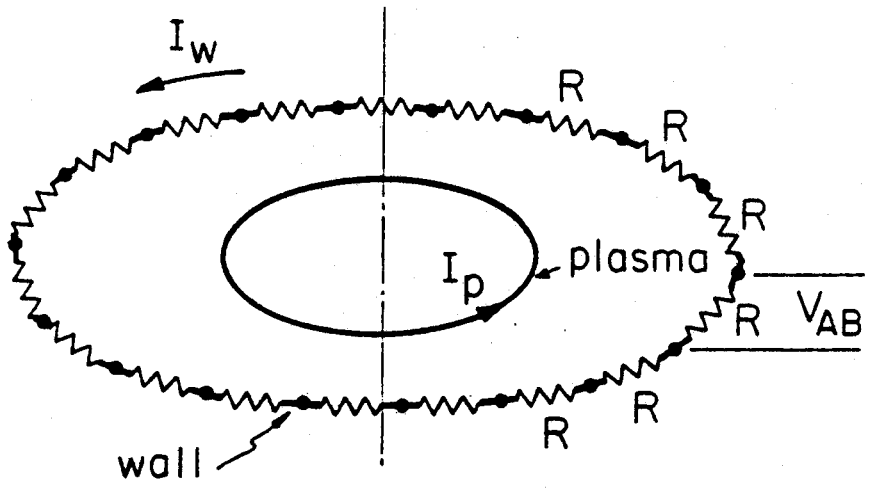

Figure 8 - When a disruption occurs, the decay of the plasma current I_p induces a current I in the conducting loop consisting of a ring of resistors.

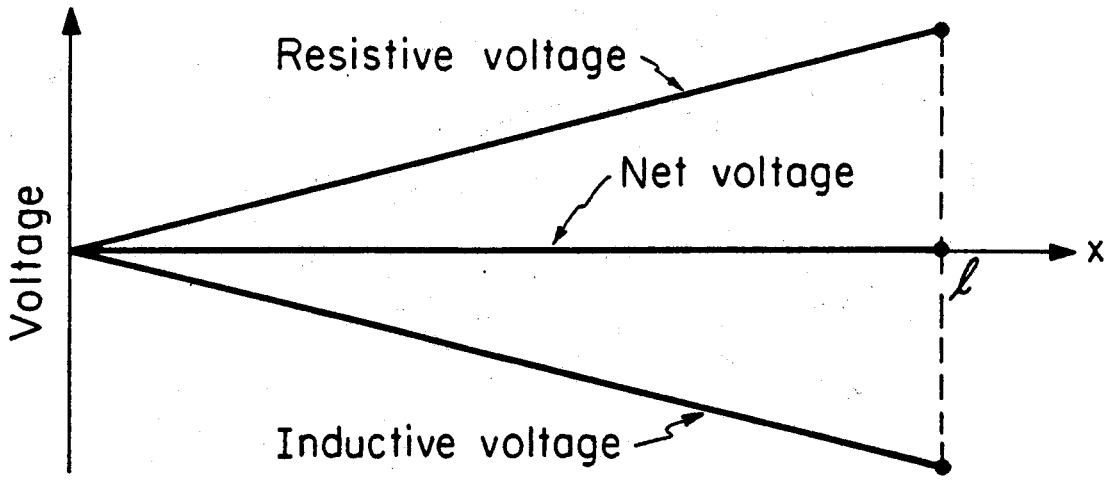

Figure 9 - The distributed inductive and resistive voltages along the ring cancel at any given instant to yield a net voltage of zero at each point.

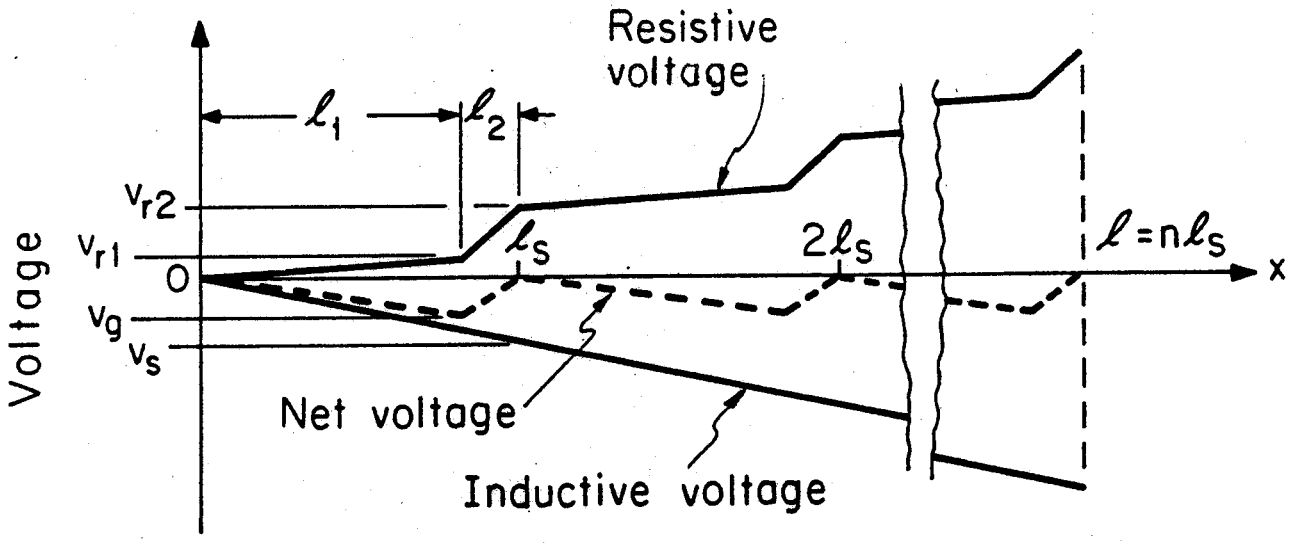

Figure 10 - Alternating high and low resistors in the ring [eg - $(R_2/\ell_2) >> (R_1/\ell_1)$] combine with the distributed inductive voltage to give a "sawtooth" net voltage at any given instant with maximum value V_g.

voltage. In this sketch, the peripheral length occupied by small and large resistors is ℓ_1 and ℓ_2, respectively. The maximum net voltage is shown as V_g. In the extreme where $\ell_2 << \ell_1$ and all of the resistance is in ℓ_2 with no resistance in ℓ_1, then V_g approaches the maximum value V_s. The latter is the indyctive voltage divided by the number of resistor pairs or segments. The manner in which this can be related to induced sector gap voltages in the event of a plasma disruption is shown in Fig. 11.

The right side of Fig. 11 is a section of the outboard region of a torus consisting of two continuous shells. The inner shell is convoluted and forms gaps of width g on the plasma side. The plasma loop current lies in the plane of the figure and is not shown. It produces some flux on the plasma side in region (1) which does not link any closed contour through a shell. This portion of the flux may be considered to collapse at the same rate as the plasma current decay. The flux ϕ_g, in the gaps is also in this category. Flux produced by the plasma which originally passes through regions such as (2) or (3) will take longer to decay since it induces currents of the type shown for the shells in Fig. 3b and for shell e in Fig. 3a.

The left side of Fig. 11 shows one pair of resistors from a closed loop and represents wall resistances for one sector of the inner shell as shown on the right. If there are n sectors (i.e. - n pairs of resistors) then the maximum voltage across the gap g occurs for $g << \ell_1$ and $(R/\ell)_1 \to 0$ in which case

$$V_{g\ max} = - \dot{\phi}/n \qquad (3)$$

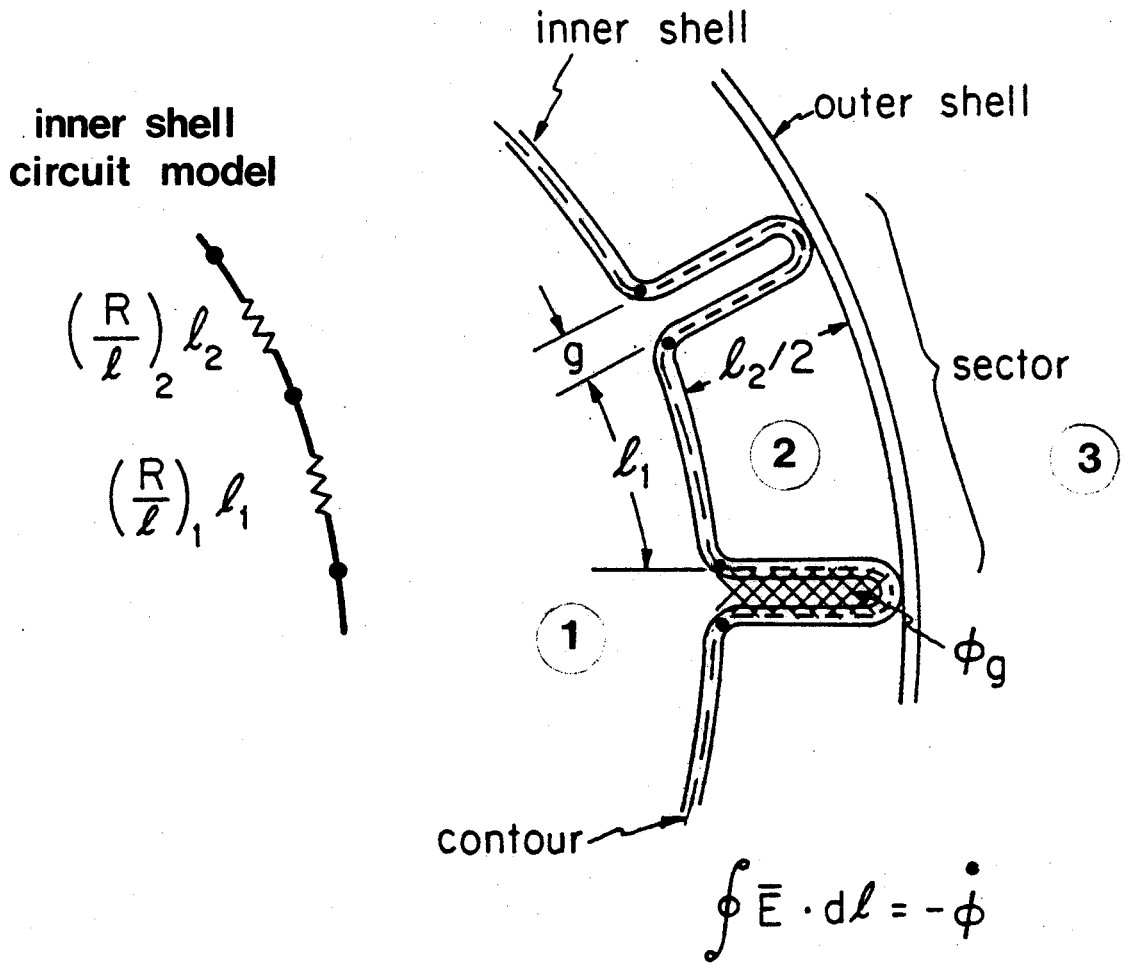

Figure 11 - Sketch of a sector inner and outer shell and the contour around the plasma side for estimation of sector gap voltages.

where $\dot{\phi}$ is the rate of change of flux through the area enclosed by the dashed contour and is also the total inductive voltage available to drive current along this path. If the wall resistances per unit length are finite for both ℓ_1 and ℓ_2 then the gap voltage for $g << \ell_1$ is given by

$$V_g = -\frac{\dot{\phi}}{n}\left[1 + \frac{(R/\ell)_1 \ell_1}{(R/\ell)_2 \ell_2}\right]^{-1} \qquad (4)$$

Equation (4) shows that the gap voltage can be reduced significantly by decreasing the resistance along the path ℓ_2 relative to that along ℓ_1. This could be done, for example, by using a lower resistivity material along or in parallel with ℓ_2 or by using a thicker wall along ℓ_2 than along ℓ_1.

The most conservative estimate for $\dot{\phi}$ for use in (3) or (4) would be to assume that all the flux initially produced by the plasma links the contour and collapses on the time scale of the plasma current decay. The flux would then be equal to $L_p I_p$ where L_p is the plasma self inductance and I_p is the plasma current. This is a conservative assumption and may be overly pessimistic because it includes a large fraction of flux which does not link the torus walls (e.g. - see shaded region in Fig. 1b). Equations (3) and (4) will be used in the next section to estimate disruption-induced gap voltages for INTOR and FED. They will be based on the computed rates of change of flux at point d (Fig. 1a) which corresponds to the gaps in the z = 0 plane on the outboard side. The examples will neglect the flux ϕ_g originally in the gaps (see Fig. 11) since this can be shown to be a small correction in these cases. In a later stage of design, the estimates should also be performed at locations other than the z = 0 plane

with further consideration of the potential impact of plasma motion and azimuthal asymmetry of the flux change.

3.2 Examples for INTOR and FED

Figures 2c and 4c to 7c provide the means for estimating $\dot{\phi}$ for any contour in the z = 0 plane for several shell configurations. The gap locations on the plasma side in this plane are at points d and b (see Fig. 1a). For the purposes of estimating voltages for FED and INTOR we shall concentrate on the flux change for a contour through d since the flux initially available at that point is greater than that for b in all cases. Note that the use of the total flux produced by the plasma (point c) would considerably overestimate that available for voltage generation in the gaps.

The model is based on a rectangular, stationary, discharging plasma of uniform current density. The overall shell dimensions in the model were comparable to those in INTOR and FED, but differ somewhat from these cases as illustrated in Fig. 12a and 12b. Exact shell dimensions must eventually be used together with a better plasma model including motion. However, the trends which are given may be expected to be correct and voltage levels to be of the proper order of magnitude.

Table 1 gives estimates based on different shell configurations as described in the figures for Section 2.0. In all cases shell thickness to resistivity ratios correspond to $\approx$ 4 cm of stainless steel. Parameters assumed for FED and INTOR are given in the footnotes. Line 1 is based on two shells which are each toroidally continuous to allow for net current

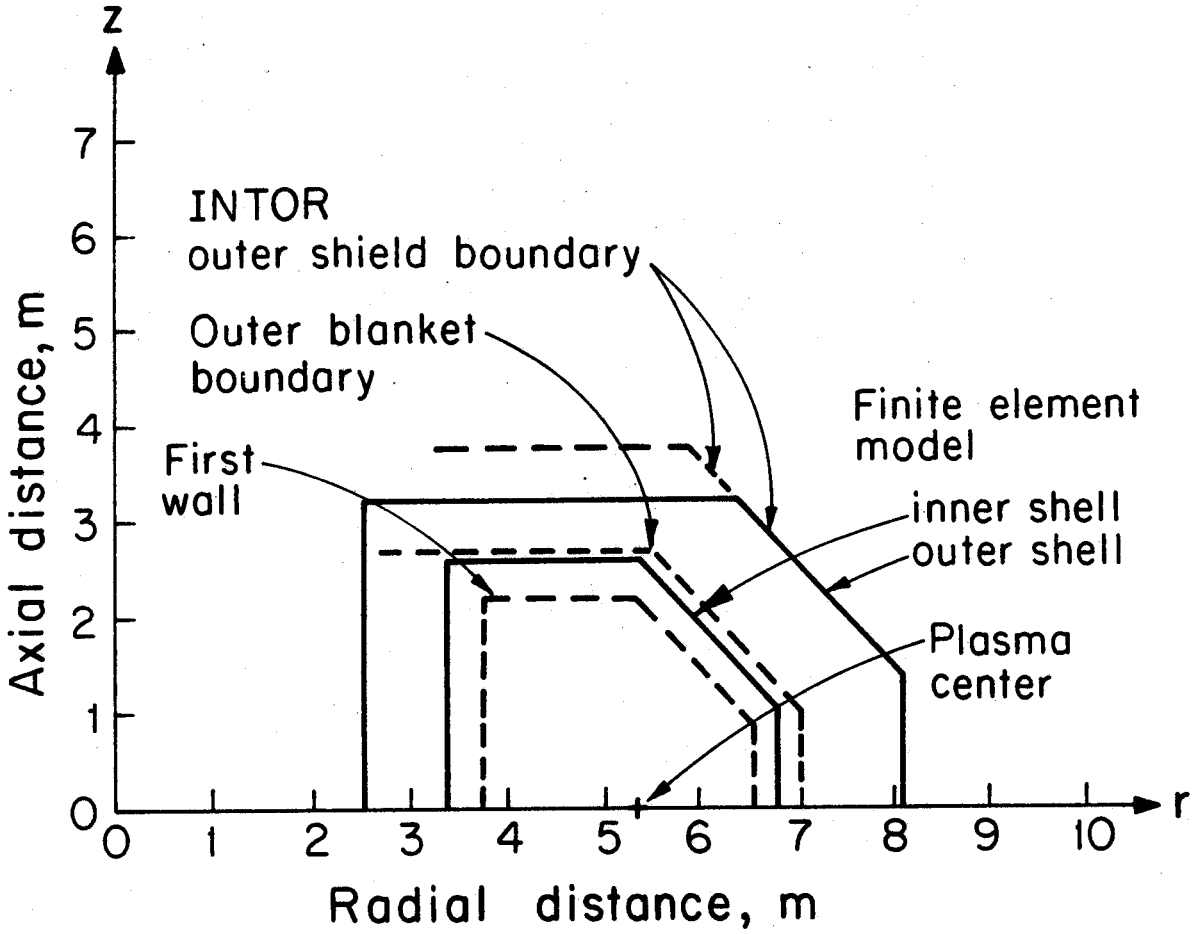

Figure 12a - Illustration of finite element model shell locations relative to the INTOR inner boundary, outer blanket boundary (assumes 0.5 m blanket), and outer shield boundary (assumes 1 m shield + 0.1 m gap).

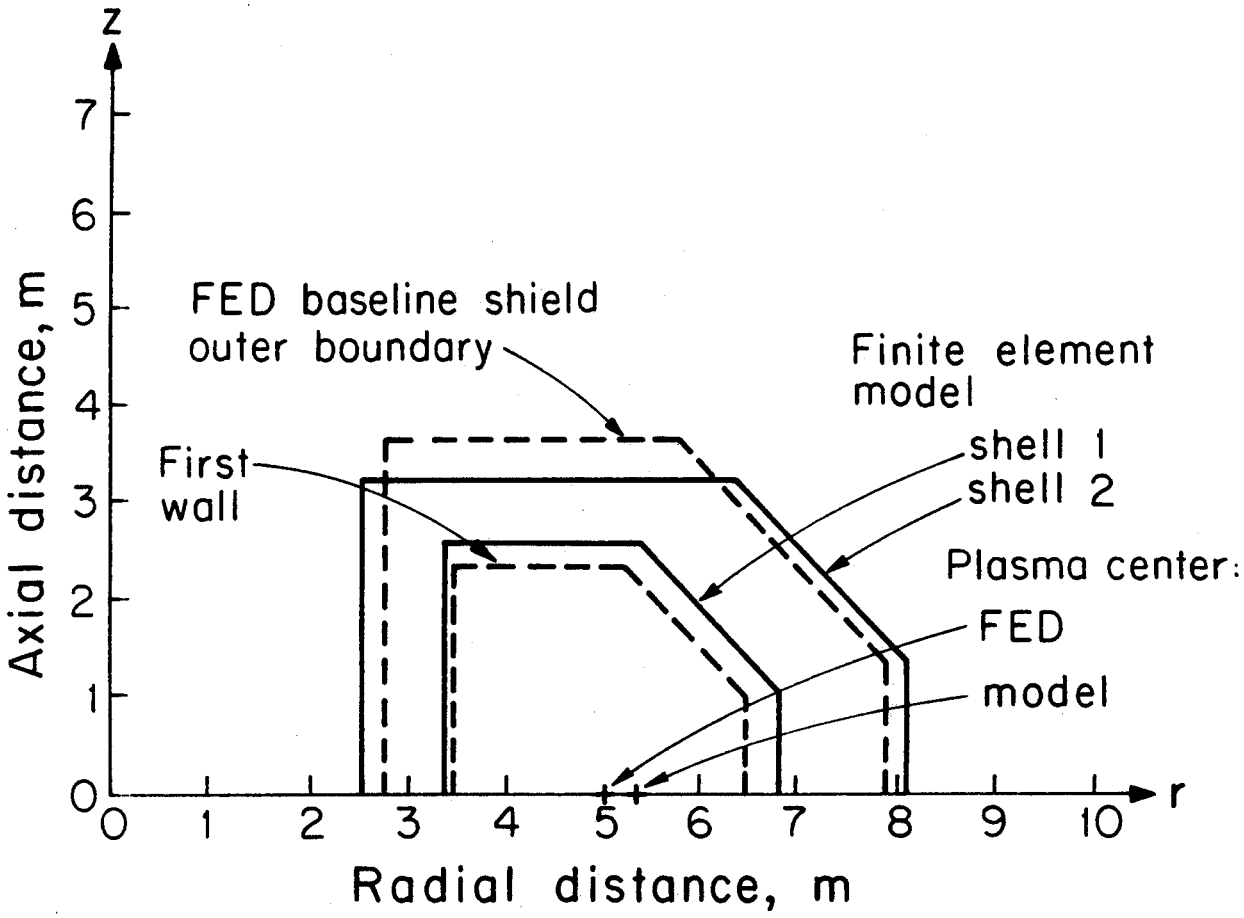

Figure 12b - Illustration of finite element model shell locations relative to the FED baseline first wall and shield outer boundary.

TABLE 1 - SECTOR GAP VOLTAGE ESTIMATES FOR INTOR AND FED FOR SELECTED SHELL CONFIGURATIONS(1)

	CONFIGURATION(2)	FIG. NO.	FED GAP(3) $V_{g\ max}$ (Volt)	FED GAP(3) V_g (Volt)	INTOR GAP(4) $V_{g\ max}$ (Volt)	INTOR GAP(4) V_g (Volt)	CASE NO.(5)
1.	2 shells with net current in each	2	61	24	30	14	10
2.	2 shells with no net current	4	216	86	107	50	18
3.	2 shells with no net current plus complete outer shell with net current	5	87	35	43	20	20
4.	2 shells with no net current plus partial shell inboard with net current	6	111	44	55	26	28
5.	2 shells with no net current plus partial shell outboard with net current	7	173	69	85	39	29

(1) estimates based on shell model shown in referenced figures in column 2

(2) all shells correspond to (shell thickness/resistivity) = $4.12 \times 10^4\ \Omega^{-1}$ (equivalent to ≈ 4 cm ss)

(3) based on 5.4 MA, 10 gaps, 10 msec discharge, $\ell_1 = 4.2$ m, $\ell_2 = 2.8$ m

(4) based on 6.4 MA, 12 gaps, 20 msec discharge, $\ell_1 = 3.46$ m, $\ell_2 = 3$ m

(5) for author reference only

flow as shown in Fig. 2. Maximum gap voltages are given in columns 3 and 5 based on Eq. (3) and gap voltages based on Eq. (4) are given in columns 4 and 6. The maximum gap voltage, $V_{g\ max}$, corresponds to the maximum inductive voltage drop per sector whereas the gap voltage, V_g, gives the net voltage across the gap on the plasma side. Estimates do not include the effect of the gap flux, ϕ_g, in Fig. 11, since it represents a minor correction for the cases considered.

Two toroidally-continuous shells (line 1) yield low voltages, but are probably not practical. The other extreme is two sectored shells which cannot provide a net current flow through an rz-plane and is considered in line 2. The last three cases correspond to two shells with no net current flow and net current flow in either a complete outer shell, partial shell inboard or partial shell outboard. Results fall within the bracket formed by the first two cases and indicate that gap voltages of the order of 30 to 50 volts for FED and 20 to 40 volts for INTOR are probably achievable if an equivalent level of toroidal electrical continuity can be provided adjacent to, but outside the outer shell, for example, in a spool or vacuum boundary.

Table 2 is similar in format to Table 1, but considers variations in the ratio of wall thickness, t_s, to resistivity, ρ. Most cases involve two shells with no net current plus a complete outer shell with net current as shown, for example, in Fig. 5. Lines 1 to 4 utilize two shells, each with an equivalent thickness to resistivity ratio corresponding to $\sim$ 4 cm of stainless steel and an outer shell corresponding to $\sim$ 9 cm, $\sim$ 4 cm, $\sim$ 2 cm and 0 cm of stainless steel, respectively. Voltage results

TABLE 2 - SECTOR GAP VOLTAGE VARIATIONS WITH OUTER SHELL THICKNESS AND RESISTIVITY[1]

CONFIGURATION	t_s/ρ [$10^4\ \Omega^{-1}$][2] SHELL 1	SHELL 2	OUTER	FED GAP[3] $V_{g\ max}$ (Volt)	FED GAP[3] V_g (Volt)	INTOR GAP[4] $V_{g\ max}$ (Volt)	INTOR GAP[4] V_g (Volt)	CASE NO.[6]
1. 2 shells with no net current plus complete outer shell with net current	4.12[5]	4.12	9.41	80	32	40	19	24
2. same as 1.	4.12	4.12	4.12	87	35	43	20	20
3. same as 1.	4.12	4.12	2,06	99	40	49	23	19
4. 2 shells with no net current	4.12	4.12	0	216	86	107	50	18
5. 2 shells with net current	4.12	4.12	0	61	24	30	14	10
6. same as 1.	1.03	1.03	1.03	173	68	85	40	27
7. shells with very high resistivity	~ 0	~ 0	~ 0	550	-	272	-	-
8. estimate based on total plasma flux	-	-	-	900	-	444	-	-

(1) estimates based on shell models of Section 2.0

(2) t_s = shell thickness; ρ = shell resistivity

(3) see footnote (3), Table 1

(4) see footnote (4), Table 1

(5) equivalent to ~ 4 cm ss

(6) for author reference only

indicate that the largest incremental decrease in voltage occurs by providing some toroidal continuity (e.g. - compare lines 3 and 4) and that little is gained by increasing the wall thickness to resistivity ratio beyond the level of $2.06 \times 10^4\ \Omega^{-1}$ for the outer shell. Two shells with net current are given in line 5 to illustrate a probable lower limit even though providing two such shells is quite difficult. Line 6 gives results equivalent to using ~ 1 cm thick stainless steel for all three shells and line 7 provides an upper limit to sector voltage since it corresponds to a case where all of the flux coupled by the contour through point d in Fig. 1a is allowed to collapse with the discharge time of the plasma. This assumption is conservative, but less conservative than the case in line 8 which assumes that all of the flux produced by the plasma (point c in Figure 2c and 4c to 7c) is available for gap voltage production.

The approach for the estimates in lines 7 and 8 can be applied following generation of a simple flux map of the $t < 0$ steady state flux produced by the plasma or, equivalently, calculation of the plasma self inductance and a coupling coefficient with a contour through the gap location. However, results will tend to be overly conservative. The approach used for the other cases in Tables 1 and 2 required a solution of the eddy current problem to find the initial $\dot{\phi}$ through the contour. This is more realistic, but still neglects the effects of plasma motion or possible asymmetrical flux changes.

The examples indicate typical voltage levels which can be expected and the considerable flexibility in control of these levels through design of wall continuity, thickness and resistivity. Before a realistic design

can be approached, however, it will be necessary to specify an allowable voltage level.

4.0 SHELL TIME CONSTANTS

The currents in the shells in the previous sections and their corresponding fields are induced by the changing plasma flux during a disruption and further decay over a time interval dependent on shell geometry, toroidal continuity, shell thickness to resistivity ratio and plasma geometry. Flux decay versus time at the plasma center is shown in Fig. 13, for selected cases. The top two curves correspond to configurations involving two shells with net current flow and two different values of t_s/ρ to show that the decay times are proportional to this parameter for cases of equivalent shell geometry, plasma geometry, and restrictions on net current flow. The lowest curve (i.e., - fastest decay) is also for a two shell situation and has the same t_s/ρ as the second curve, but shows a dramatically different decay time because it is a "no net current" case. From a circuit standpoint, "net current" and "no-net current" may be envisioned as conditions which significantly alter the coupling coefficients among the shells and plasma and, in turn, the circuit time constants. The third curve consists of two shells with no net current and a third, complete, outer shell capable of carrying net current. This case is also considered in Fig. 14 where the (t_s/ρ) for two shells with no net current is held constant and $(t_s/\rho)_o$, the value for the outer shell, is allowed to vary. The trend in decay time is as would be expected, but time scaling proportional to $(t_s/\rho)_o$ is not valid since (t_s/ρ) for <u>all</u> shells was not

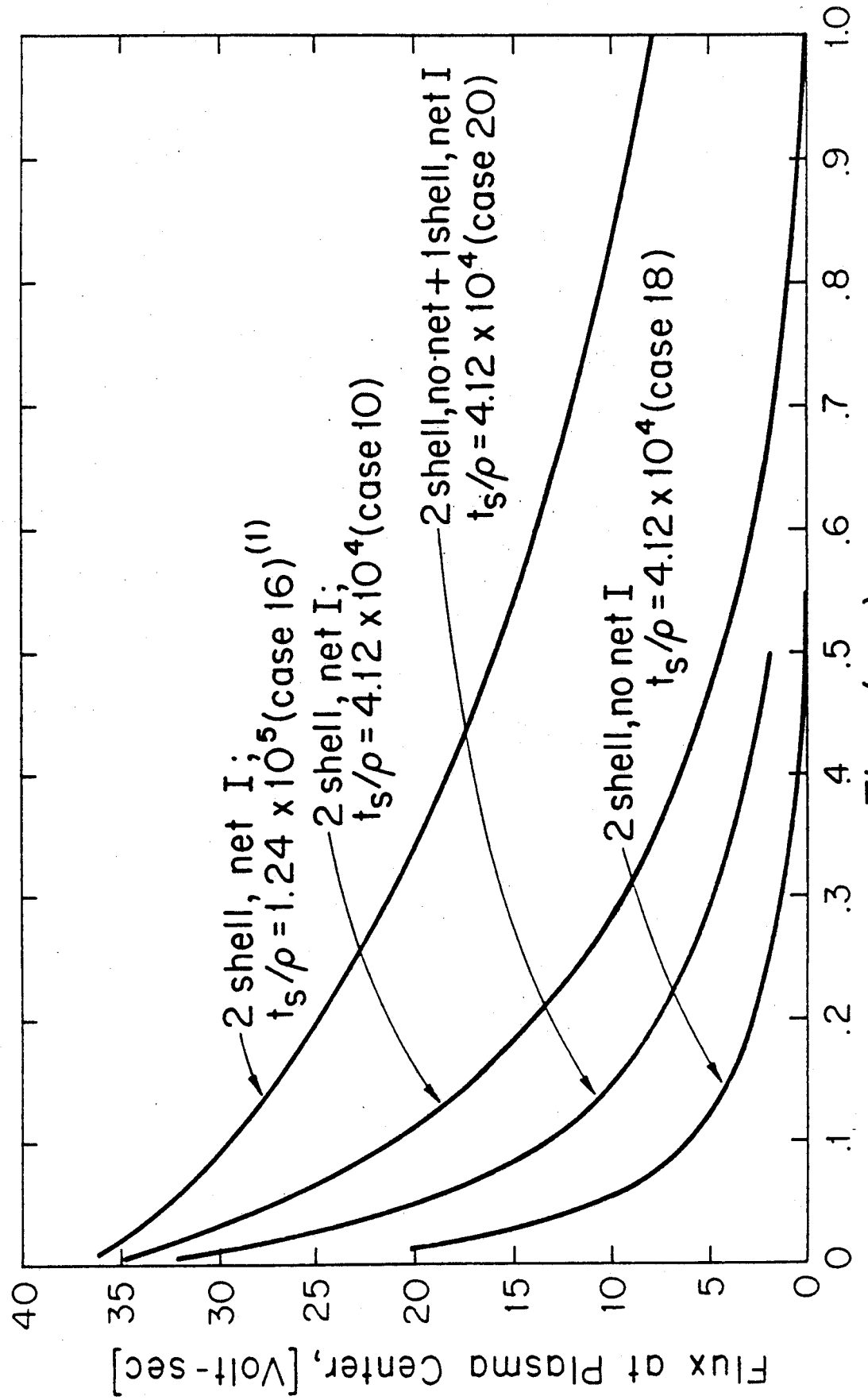

Figure 13 - Flux Decay at the Plasma Center for Selected Cases.

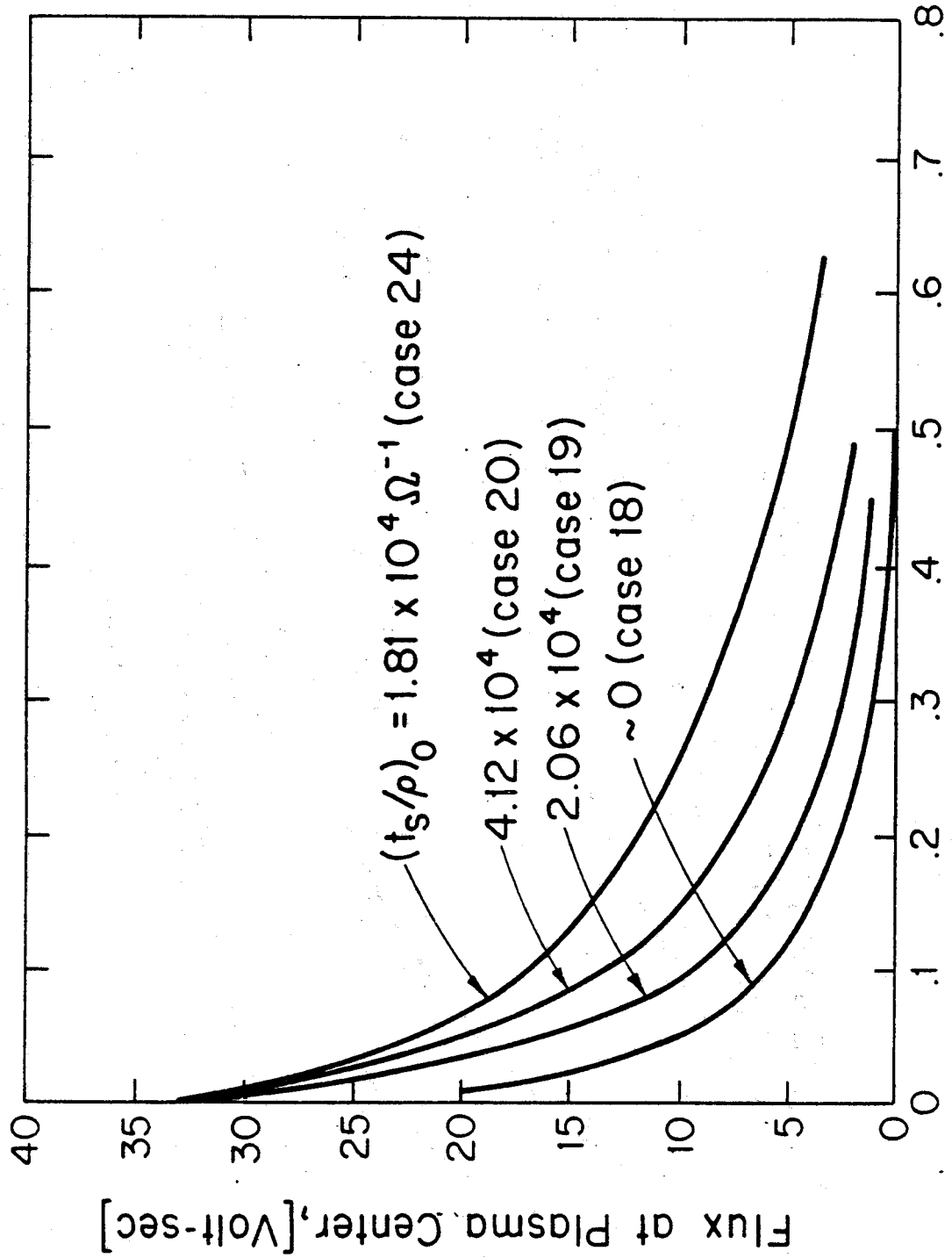

Figure 14 - Flux Decay at the Plasma Center for Two Shells with no net current ($t_s/\rho = 4.12 \times 10^4\ \Omega^{-1}$) and an outer shell with net current and selected cases of $(t_s/\rho)_o = (t_s/\rho)_{outer}$.

changed proportionally.

Finally, it should be noted that all curves indicate a monotonic decay in time which cannot be described by a single exponential time constant. The initially induced current distribution may be envisioned as a fundamental with higher order harmonics where the amplitudes are dependent on shell geometry, resistivities, and plasma current distribution. The highest order harmonics decay first, but at any given instant the decay is governed by a combination of "time constants". This is illustrated in Fig. 15 where the instantaneous decay time for induced field energy is plotted as a function of time for three cases. The decay time at any instant is given by

$$\tau_e = \frac{2E_i}{\dot{E}_i} \tag{5}$$

where: E_i = energy associated with induced field

$\dot{E}_i$ = instantaneous rate of change of E_i

In each case τ_e rises initially then levels off after the higher order harmonics in the current distribution decay to a fundamental. The final values of τ_e are not directly scalable to $(t_s/\rho)_o$ since all shells were not scaled in the same proportion.

This section has discussed the induced field decay time associated with many of the cases in Section 2.0. Results indicate that considerable flexibility exists for adjustment of these rates. For a fixed shell geometry and set of restrictions on net current flow, decay times may be scaled proportional to the ratio of shell thickness to resistivity. Scaling does not apply if only a portion of shell components are altered, however.

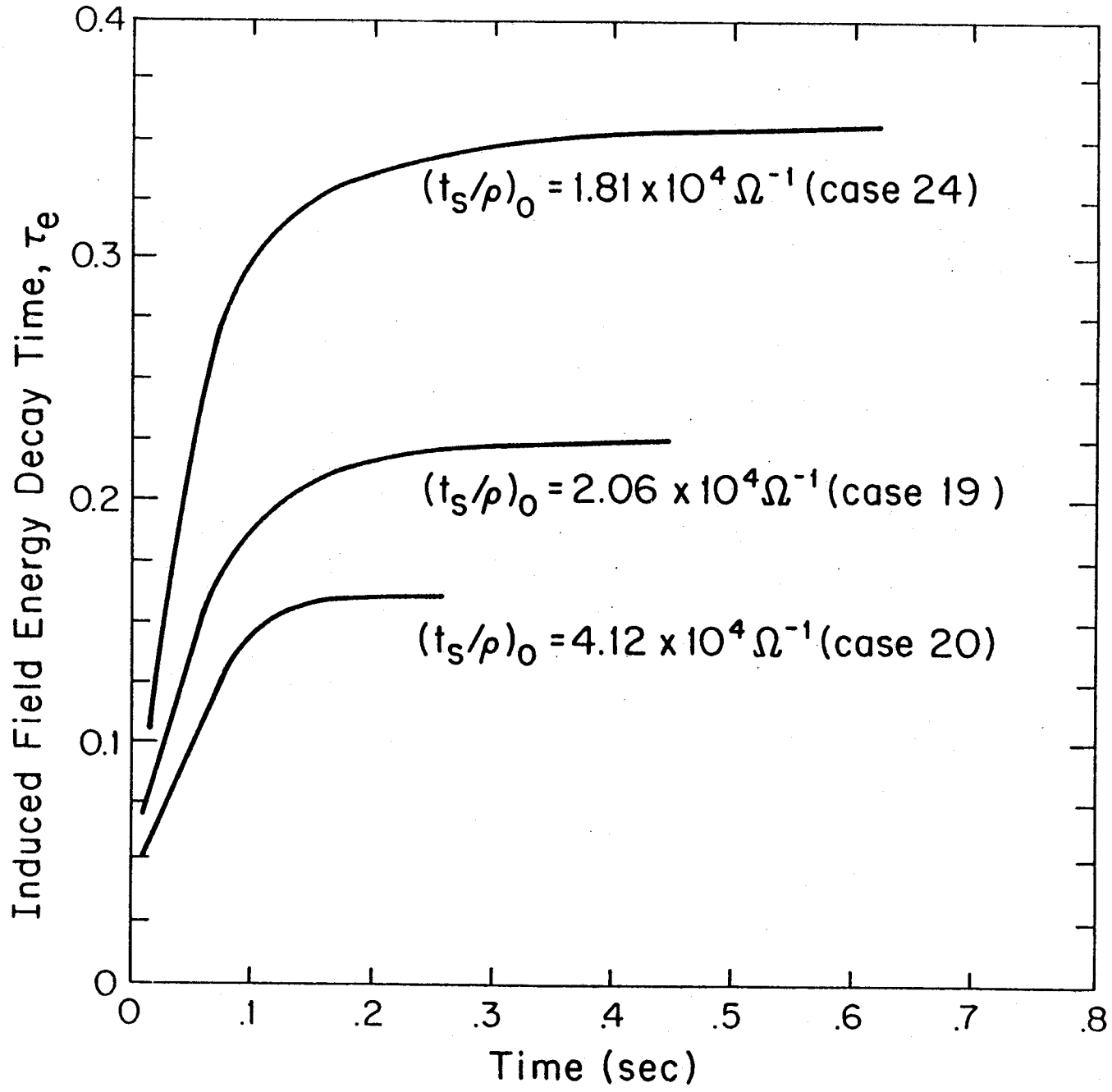

Figure 15 - Induced Field Energy Decay Time for two shells with no net current $(t_s/\rho) = 4.12 \times 10^4\ \Omega^{-1}$ and a complete outer shell with selected values of $(t_s/\rho)_o$

5.0 EDDY CURRENT LOADS ON SECTORS

The toroidal currents induced in the shells when a plasma disruption occurs must flow between shells at the ends of the sectors if the shells are segmented, thus requiring no net current through an rz-plane as illustrated in Fig. 3b. The currents are shown schematically in Fig. 16 which indicates that they can be considered locally as currents with components transferring between shells or components in the saddle direction. The currents have the same magnitude, but are opposite in sense in the other sector end plate. The interaction of these currents with the toroidal field leads to a net torque T, on each sector end plate which is balanced thus yielding no net moment about the plasma axis. The interaction also leads to a net z-directed force, F_z, on each end plate which produces a net overturning moment on the sector.

As an example, Fig. 17 shows the currents in the saddle direction and in the transverse direction (note the difference in scale) at 0.010 s after disruption for the case of two shells with no net current and a complete shell capable of net current flow (case 20 in the previous sections). The saddle current distribution around the end plate is shown in Fig. 18 for selected instants of time. The saddle currents are the primary source of the force, F_z, on each end plate which leads to the net overturning moment on the sector. The decay of this force in time is shown in Fig. 19 which indicates that it persists for about the same time as the currents in Fig. 18.

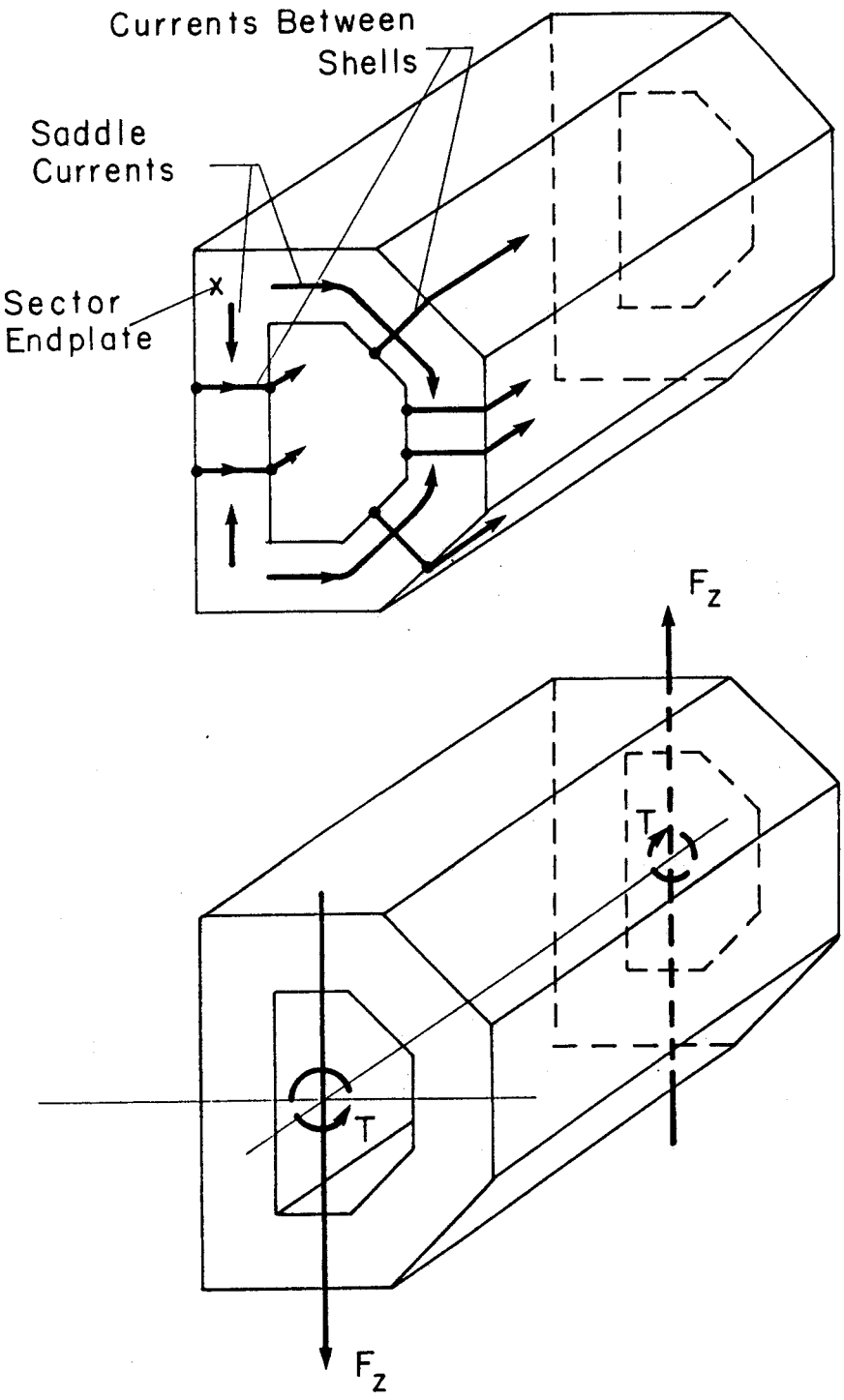

Figure 16 Induced currents which flow along the shells following a disruption transfer between shells and also flow in the saddle direction in the sector end plates. The currents lead to a net z-directed force on each face which yields a net overturning moment. In addition, a torque is generated on each face, but does not yield a net moment on the sector.

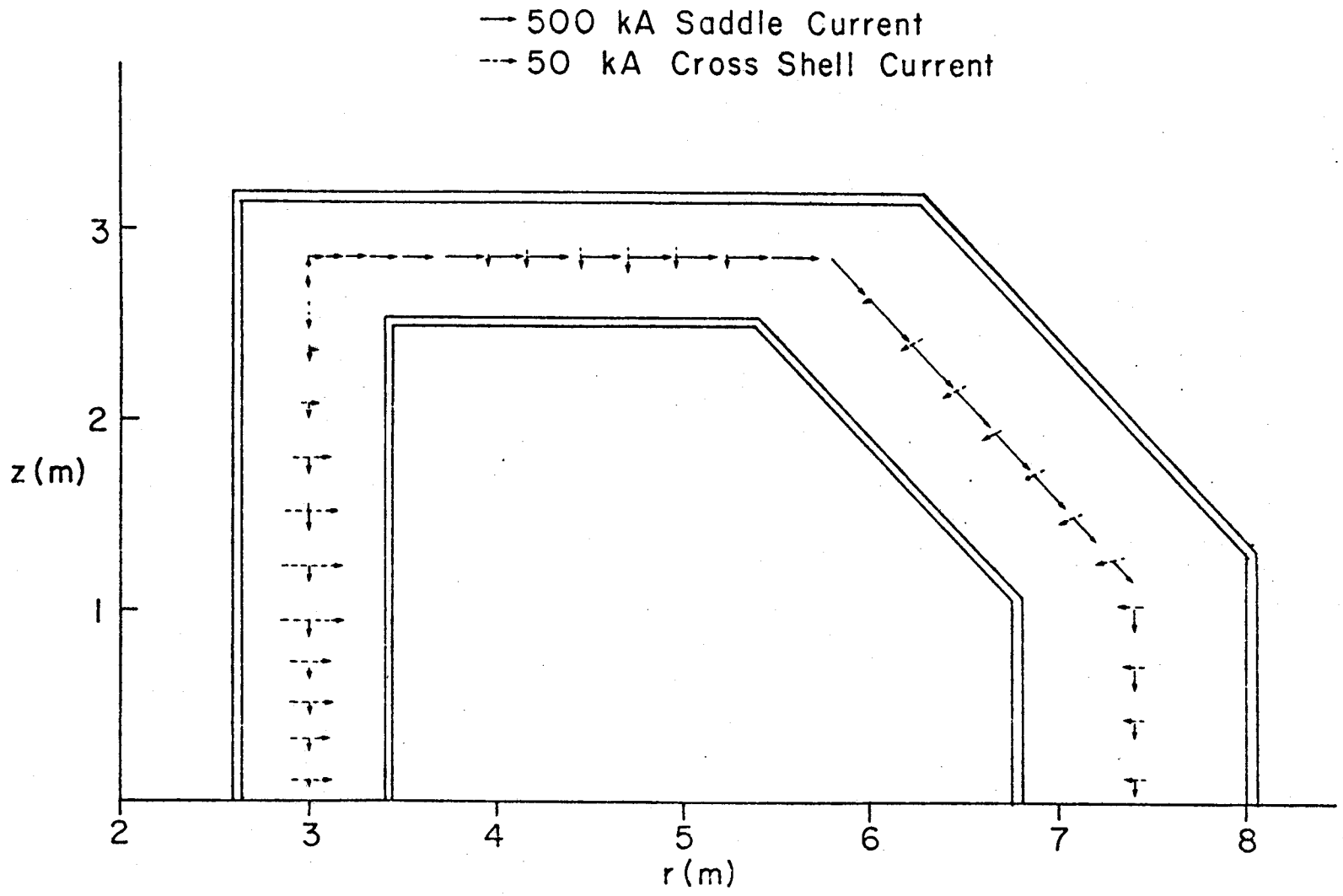

Figure 17 Saddle currents and currents between shells in one sector end plate 0.010 sec after disruption (Case 20).

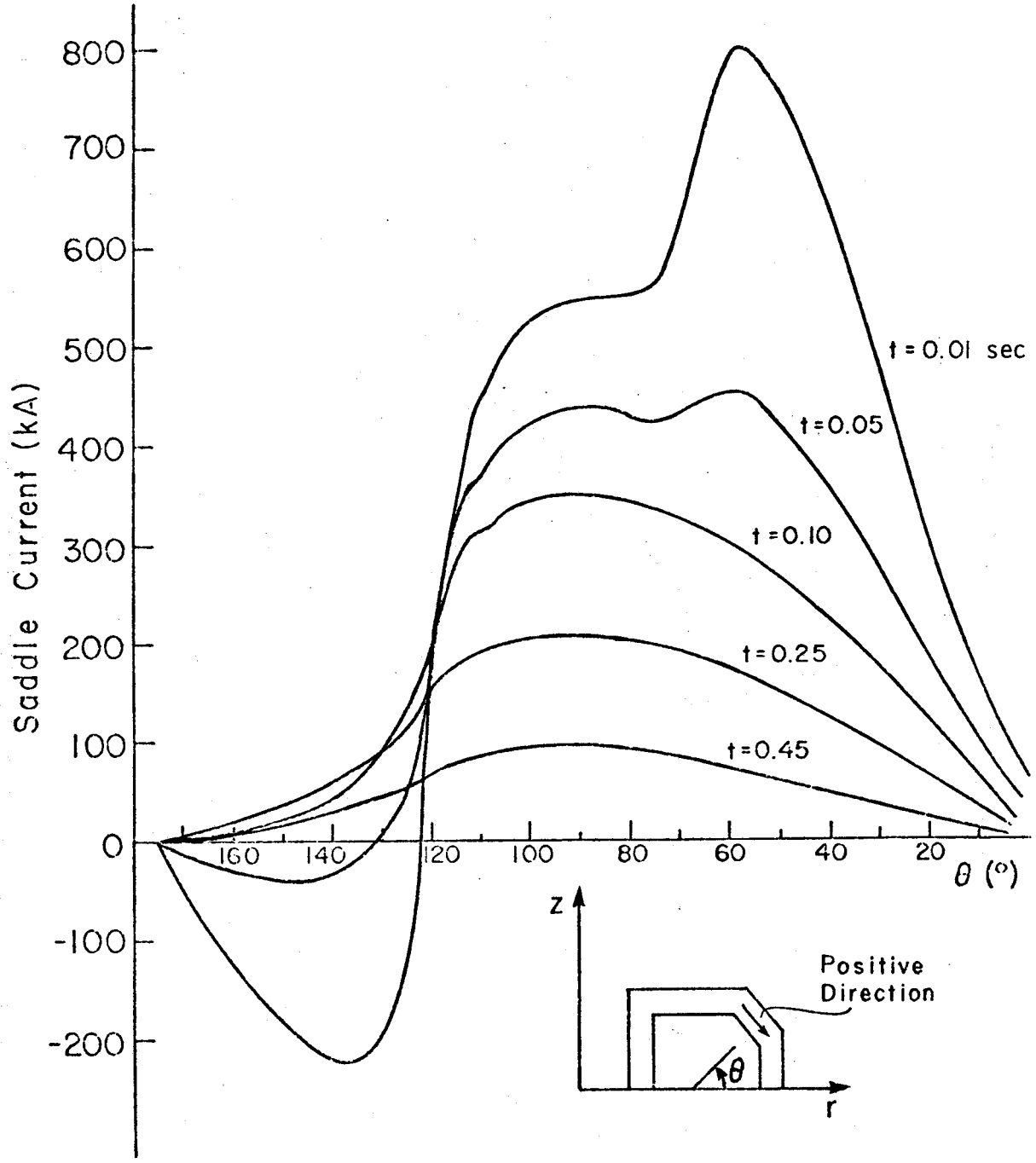

Figure 18 Saddle Current Distribution in the Sector End Plate at Selected Instants After Disruption (Case 20).

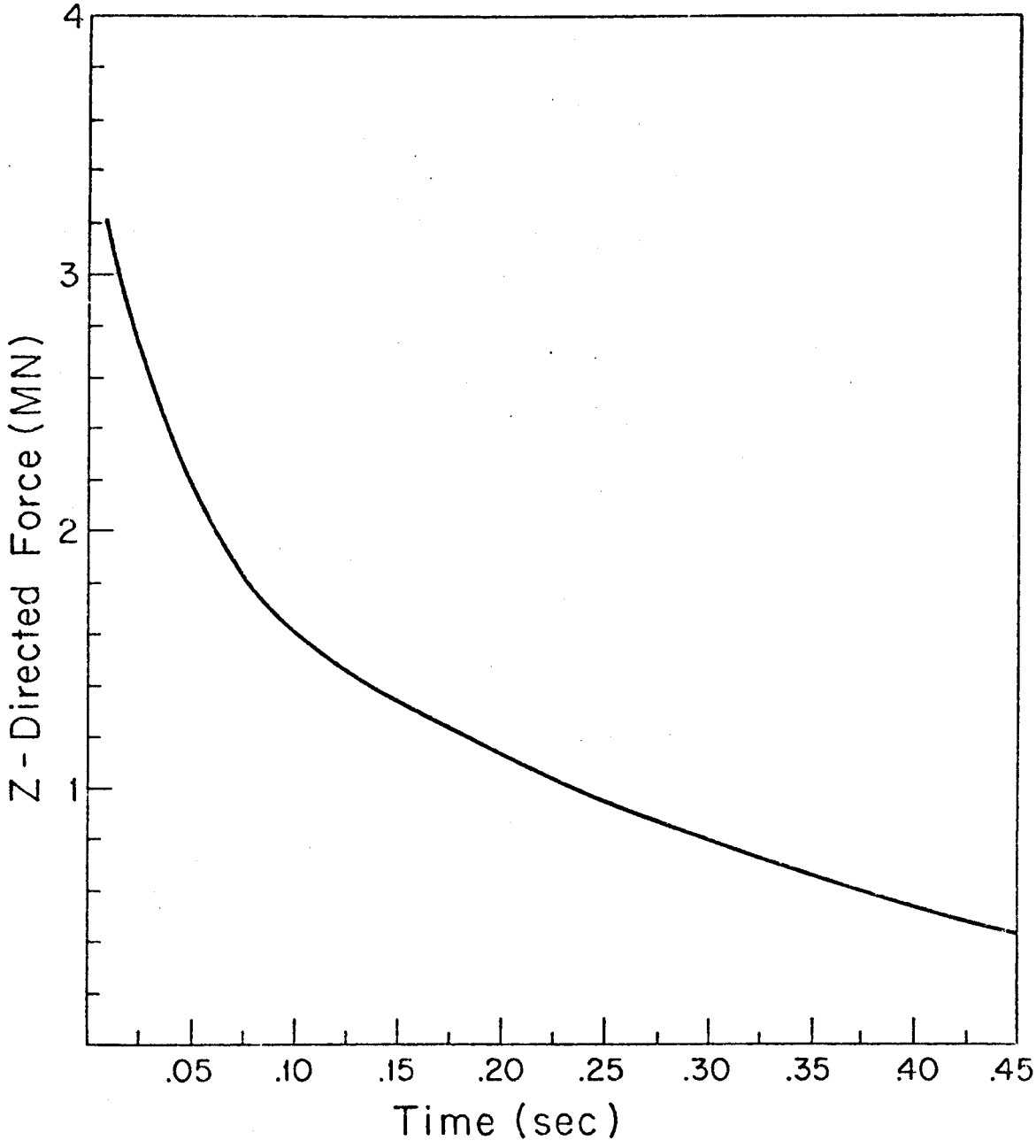

Figure 19 Total Z-Directed Force on Sector End Versus Time (Case 20) ($F_z \propto I_p$; I_p = 5.4 MA).

The "no net" torque, T, on each end plate is plotted versus time in Fig. 20. This torque decays more rapidly because its primary source is the current transfer between shells which would be expected to have a sborter time constant than the saddle currents.

The purpose of this section was to illustrate the type of eddy current patterns and loads which can be expected in a sector following a plasma disruption. Typical values were generated based on dimensions comparable to FED/INTOR and indicate that the load levels are nontrivial, but have magnitudes which are feasible for support.

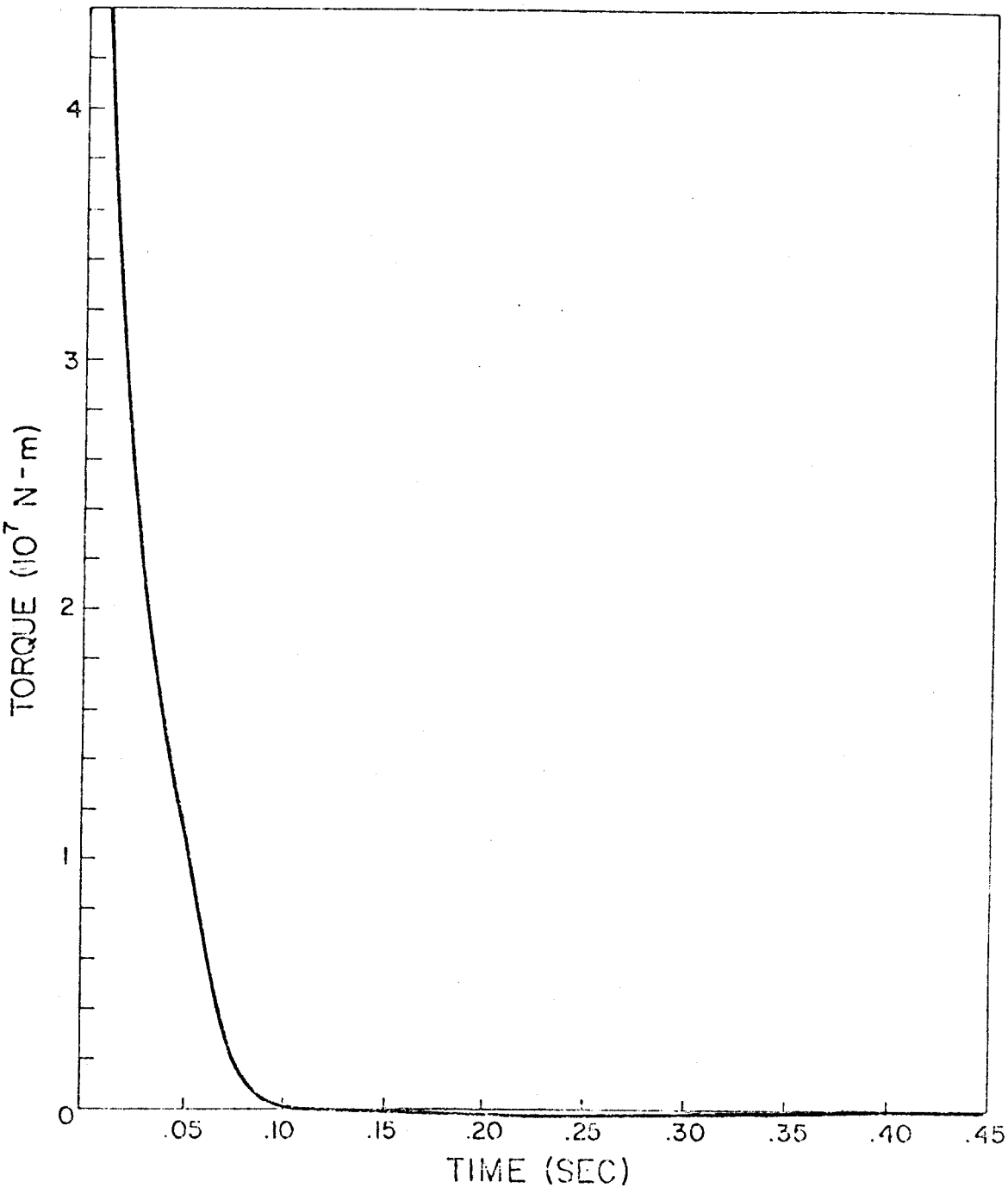

Figure 20 Torque Acting on Sector End Versus Time (Case 20).

REFERENCES

1. W.M. Stacey, Jr., M.S. Abdou, D.B. Montgomery, et al., "FED-INTOR Critical Issues - Vol. II", USA FED-INTOR/82-1, October 82.

2. R.D. Pillsbury, "A Two-Dimensional Planar or Axisymmetric Finite Element Program for the Solution of Transient or Steady, Linear or Nonlinear, Magnetic Field Problems," COMPUMAG, Chicago, September 1981.

3. R.J. Thome and J.M. Tarrh, MHD and Fusion Magnets:Field and Force Design Concepts, Wiley-Interscience, New York, 1982, Chapter 5.

4. C.A. Flanagan, D. Steiner, G.E. Smith, et al., "Fusion Engineering Device Design Description - Vol. I and II," ORNL/TM-7948/V1 and V2, December 1981.

MIT PLASMA FUSION CENTER TECHNOLOGY DISTRIBUTION LIST

AEB, Plasma Physics Division, South Africa, De Villiers, Johan
AMPC Inc., Guest, Dr. G.
Association Euratom - CEA, Dept. de Physique de Plasma et de la Fusion Controle, France
Australian National University, Australia, Hamberger, S.M.
Bank of Tokyo, Ltd., Japan, Azuma, Mr. Katsuhiko
Brookhaven National Laboratory, Powell, James R.
Central Research Institute for Physics, Hungary, Kostka, P.
Chalmers University of Technology, Sweden, Wilhelmsson, K.H.B.
CNEN - Centro di Frascati, Italy
CNR - Centro di Studio sui Gas Ionizzati, Italy, Ortolani, S.
Consoli, T., France
Culham Laboratory, United Kingdom, Wesson, J.A.
Division of Research and Laboratories, Austria, Frolov, V.
Ecole Royale Militaire, Belgium, Vandenplas, P.E.
EG&G Idaho, Inc., Crocker, Mr. J.
Electrical Power Research Institute, Ambeard, Dr. Noel
FOM-Institute for Plasma Physics, Rijnhuizen, Netherlands
General Atomic Company
Georgia Institute of Technology, Stacey, Jr., Dr. W.M.
ITT, India, Tewari, Prof. D.P.
Inst. of Physics, Warsaw University Branch, Poland, Brzosko, J.S.
Inst. Nacional de Invest. Nucleares, Mexico, Ramos Salas, J.S.
Japan Atomic Energy Research Institute, Japan, Mori, Dr. S.
JET Joint Undertaking, United Kingdom
KFA Julich, Institut fur Plasmaphysik, FRG
Kurchatov Institute of Atomic Energy, USSR
Lawrence Berkeley Laboratory, Sessler, Dr. A.M.
Lawrence Livermore Laboratory, Alira, Richard
Lebedev Institute of Physics, USSR, Rabinovich, Dr. M.S.
Los Alamos Scientific Laboratory, CTR Division
Max-Planck-Institute fur Plasmaphysik, FRG
Naval Research Laboratory, Granatstein, Dr. Victor
New York University, Courant Inst. of Mathematical Sci., Grad, Prof H.
Nuclear Research Institute, Czechoslovakia, Bartosek, V.
Oak Ridge National Laboratory, Fusion Energy Division
Oak Ridge National Laboratory, Peng, Y-K. M.
Osaka University, Japan, Ito, H.
Palumbo, D., Belgium
Princeton University, Princeton Plasma Physics Laboratory
Rijksuniversiteit Gent, Belgium, Verheest, F.
Riso National Laboratory, Denmark, Jensen, V.O.
Royal Institute of Technology, Sweden, Lehnert, B.P.
Ruhr-Universitat, FRG, H-J. Kunze
S. Kaliski Inst. of Plasma Phys. and Laser Microfusion, Poland, Fiedorowicz, H.
Sandia Research Laboratories, Yonas, Dr. Jerry
Science Applications, Inc., MD, Dean, Dr. Stephen
Science Council of Japan, Japan, Fushimi, K.
Siberian Section of the USSR Academy of Sciences, USSR, Ryutov, Dr. D.D.
Soreq Nuclear Research Center, Israel, Rosenblum, M.
Stanford University, Buneman, Prof. O.
Technion, Israel, Rosenau, P.
Tel-Aviv University, Israel, Cuperman, S.
TRW Defense and Space Systems, Lazar, Dr. Norman
U.S. Department of Energy, Office of Fusion Energy
U.S. Department of Energy, Kostoff, Dr. Ronald N.
U.S. Department of Energy, Thomasson, Dr. Neil
U.S. Department of Energy, Trivelpiece, Dr. A.W.
Universitat Innsbruck, Austria, Cap, F.
Universitat Stuttgart, FRG, Wilhelm, R.
Universite de Montreal, Canada, Paquette, G.
Universite Libre de Bruxelles, Belgium, Balescu, R.C.
University of Alberta, Canada, Offenberger, A.A.
University of Bergen, Norway, G. Berge
University of British Columbia, Canada, Curzon, Dr. F.
University of California at Berkeley, Kunkel, Prof. W.
University of California at Berkeley, Lichtenberg, Prof. A.
University of California at Irvine
University of California at L.A., Dept. of Engineering Science
University of California at San Diego, Dept. of Physics
University of Malay, Malaysia, Lee, S.
University of Maryland, Department of Physics
University of Nairobi, Kenya, Malo, J.O.
University of Natal, South Africa, Hellberg, M.A.
University of Rochester, Simon, Prof. Albert
University of Saskatchewan, Canada, Hirose, A.
University of Texas, Dept. of Physics
University of Texas, Kochanski, Dr. Ted
University of Waikato, New Zealand, Hosking, R.J.
University of Washington, Vlases, Dr. George
University of Wisconsin:
    Department of Physics
    Nuclear Engineering Department
Varian
Yale University, Hirshfield, Prof. J.

PFC BASE MAILING LIST

Argonne National Laboratory, TIS, Reports Section
Associazione EURATOM - CNEN Fusione, Italy, The Librarian
Battelle-Pacific Northwest Laboratory, Technical Info Center
Brookhaven National Laboratory, Research Library
Central Research Institute for Physics, Hungary, Preprint Library
Chinese Academy of Sciences, China, The Library
The Flinders University of S.A., Australia, Jones, Prof. I.R.
General Atomic Co., Library
General Atomic Co., Overskei, Dr. D.
International Atomic Energy Agency, Austria,
Israel Atomic Energy Commission, Soreq Nucl. Res. Ctr., Israel
Kernforschungsanlage Julich, FRG, Zentralbibliothek
Kyushu University, Japan, Library
Lawrence Berkeley Laboratory, Library
Lawrence Livermore Laborary, Technical Info Center
Max-Planck-Institut fur Plasma Physik, FRG, Main Library
Nagoya University, Institute of Plasma Physics, Japan
Oak Ridge National Laboratory, Fusion Energy Div. Library
Oak Ridge National Laboratory, Derby, Roger

Physical Research Laboratory, India, Sen, Dr. Abhijit
Princeton University, PPL Library
Rensselaer Polytechnic Institute, Plasma Dynamics Lab.
South African Atomic Energy Board, S. Africa, Hayzen, Dr. A.
UKAEA, Culham Laboratory, United Kingdom, Librarian
US Department of Energy, DOE Library
Universite de Montreal, Lab. de Physique des Plasmas, Canada
University of Innsbruck, Inst. of Theoretical Physics, Austria
University of Saskatchewan, Plasma Physics Lab., Canada
University of Sydney, Wills Plasma Physics Dept., Australia
University of Texas at Austin, Fusion Res. Ctr., Library
University of Wisconsin, Nucl. Eng. Dept., UW Fusion Library

INTERNAL MAILINGS

MIT Libraries
Industrial Liaison Office
G. Bekefi, A. Bers, D. Cohn, B. Coppi, R.C. Davidson,
T. Dupree, S. Foner, J. Freidberg, M.O. Hoenig, M. Kazimi,
L. Lidsky, E. Marmar, J. McCune, J. Meyer, D.B. Montgomery,
J. Moses, D. Pappas, R.R. Parker, N.T. Pierce, P. Politzer,
M. Porkolab, R. Post, H. Praddaude, D. Rose, J.C. Rose,
R.M. Rose, B.B. Schwartz, L.D. Smullin, R. Temkin, P. Wolff,
T-F. Yang